

RECEIVED: July 28, 2022

REVISED: September 22, 2022

ACCEPTED: September 29, 2022

PUBLISHED: October 10, 2022

Study of the Roberge-Weiss phase caused by external uniform classical electric field using lattice QCD approach

Ji-Chong Yang, Xiao-Ting Chang and Jian-Xing Chen

*Department of Physics, Liaoning Normal University,
No. 850 Huanghe Road, Dalian 116029, P.R. China*

*Center for Theoretical and Experimental High Energy Physics, Liaoning Normal University,
No. 850 Huanghe Road, Dalian 116029, P.R. China*

E-mail: yangjichong@lnnu.edu.cn, cxtinglins@163.com,
13614090213@163.com

ABSTRACT: The effect of an external electric field on the quark matter is an important question due to the presence of strong electric fields in heavy ion collisions. In the lattice QCD approach, the case of a real electric field suffers from the ‘sign problem’, and a classical electric field is often used similar as the case of chemical potential. Interestingly, in axial gauge a uniform classical electric field actually can correspond to an inhomogeneous imaginary chemical potential that varies with coordinate. On the other hand, with imaginary chemical potential, Roberge-Weiss (R-W) phase transition occurs. In this work, the case of a uniform classical electric field is studied by using lattice QCD approach, with the emphasis on the properties of the R-W phase. Novel phenomena show up at high temperatures. It is found that, the chiral condensation oscillates with z at high temperatures, and so is the absolute value of the Polyakov loop. It is verified that the charge density also oscillates with z at high temperatures. The Polyakov loop can be described by an ansatz $A_p + \sum_{q=u,d} C_q \exp(L_\tau Q_q i a z e E_z)$, where A_p is a complex number and $C_d > 0, C_u \geq 0$ are real numbers that are fitted for different temperatures and electric field strengths. As a consequence, the behavior of the phase of Polyakov loop is different depending on whether the Polyakov loop encloses the origin, which implies a possible phase transition.

KEYWORDS: Lattice QCD, Phase Diagram or Equation of State, Phase Transitions

ARXIV EPRINT: [2207.11796](https://arxiv.org/abs/2207.11796)

Contents

1	Introduction	1
2	External electric field	2
3	Numerical results	4
3.1	Matching	4
3.2	Chiral condensation	6
3.2.1	The Z distribution of chiral condensation	6
3.2.2	The fitting of chiral condensation	8
3.2.3	The chiral condensation as a function of electric field strength	12
3.2.4	The charge distribution	15
3.3	Polyakov loop	16
3.3.1	The properties of Polyakov loop	17
3.3.2	An ansatz for the Polyakov loop	21
3.3.3	A criterion to distinguish the different behaviors of the Polyakov loop	24
4	Summary	28

1 Introduction

The study of Quantum Chromodynamics (QCD) matter is essential for a deeper understanding of the nature of strong interactions. In recent years, the effects of electromagnetic fields have also become a hot topic due to the strong electromagnetic fields that can be generated in heavy ion collision experiments [1–6]. The effect of electromagnetic field on chiral condensation has been investigated by using various low-energy effective models [7–11], which shows that the magnetic field may induce magnetic catalysis. However, inverse catalysis is observed around pseudo critical temperature [12] in the lattice calculation, and then the presence of an external magnetic field is investigated intensively in both lattice approach [5, 13–19, 19, 20] and using effective models [21–31]. By now the community has developed a good understanding of inverse magnetic catalysis, but there is still no theory that can explain all the phenomena observed in lattice simulations at one time, for example the phenomena with respect to diamagnetism, paramagnetism, meson mass, meson condensation, etc.

Not only magnetic fields but also strong electric fields are generated in non-central high-energy heavy ion collisions [32–34], which can reach as large as about $10m_\pi^2$, where m_π is the pion mass. In the electric field case, it has been shown that, the external electric field restores the chiral symmetry [7, 35–40]. In the lattice QCD approach, the case of an external real (Minkowski) electric field suffers from the notorious ‘sign problem’, except for

the case of isospin electric charges [41]. Similar as the case of chemical potential [42, 43], the analytical extension is often used to study the external electric field, which is also known as Euclidean electric field, or classical electric field [44–46]. In the previous studies on hadron electromagnetic polarizabilities [47–49], lattice QCD with an external electric field has been shown to be a reliable tool. The electric susceptibility is also studied with the presence an external classical electric field [50], and it is found that a non-constant charge distribution is required to maintain equilibrium [51].

Another interesting phenomena connecting the case of external classical electric field and the case of imaginary chemical potential is the presence of Roberge-Weiss (R-W) transition [52], which has been investigated by using lattice QCD approach [53]. In fact, except for the boundary, a uniform (homogeneous) static external classical electric field in axial gauge is equivalent to an inhomogeneous imaginary chemical potential. Since the case of a homogeneous imaginary chemical potential and the corresponding R-W transition has been verified in the lattice QCD approach, and a uniform external classical electric field corresponds to the case of imaginary chemical potential which varies according to coordinates linearly, the presence of the R-W transition is also expected in the case of external classical electric field. A phase transition similar to the R-W transition in the presence of fermionic fields coupled to magnetic backgrounds is studied [54].

In this work, the effect of a strong external uniform classical electric field is studied by using the lattice QCD approach, with the emphasis on the R-W phase caused by the external electric field. The case of $N_f = 1 + 1$ Kogut-Susskind staggered fermions with the same bare mass and different electric charges are investigated. The chiral condensation and charge distribution are also investigated.

The remained of this paper is organized as follows. In section 2, the model with a uniform external electric field is presented, and the connection between the electric field and imaginary chemical potential is discussed. The numerical results are established in section 3. Section 4 is a summary.

2 External electric field

Considering an external electric field at \mathbf{z} direction, $\mathbf{E} = (0, 0, E_z)$, in the axial gauge $A_z^{\text{EM}} = 0$, the gauge field can be written as $A_\mu^{\text{EM}} = (-E_z z, 0, 0, 0)$ such that $\mathbf{E} = (F_{tx}^{\text{EM}}, F_{ty}^{\text{EM}}, F_{tz}^{\text{EM}})$ where $F_{\mu\nu}^{\text{EM}} = \partial_\mu A_\nu^{\text{EM}} - \partial_\nu A_\mu^{\text{EM}}$, the superscript ‘EM’ is added to distinguish with the QCD gauge field. The Lagrangian with one massless fermion is

$$\mathcal{L}_q = \bar{\psi}_q \not{\partial}_\mu \psi_q + \bar{\psi}_q i \not{A} \psi_q - i Q_q e E_z z \bar{\psi}_q \gamma_0 \psi_q, \quad (2.1)$$

where $A_\mu = g \sum_a T^a A_\mu^a$ is the QCD gauge field, Q_q is the electric charge of the fermion.

A Wick rotation is performed to put the Lagrangian into a Euclidean space which applies a substitution that $t \rightarrow -i\tau$, $\partial_t \rightarrow i\partial_\tau$, $A_0 \rightarrow iA_4$ and $A_0^{\text{EM}} \rightarrow iA_4^{\text{EM}}$, so that

$$\int d^4x \mathcal{L}_q \rightarrow S_q = \int d^4x^E \left(\bar{\psi} \sum_{j=1}^4 \gamma_j^E \partial_j \psi + \sum_{j=1}^4 \bar{\psi} i g \gamma_j^E A_j \psi - i Q_q e E_z z \bar{\psi} \gamma_4^E \psi \right), \quad (2.2)$$

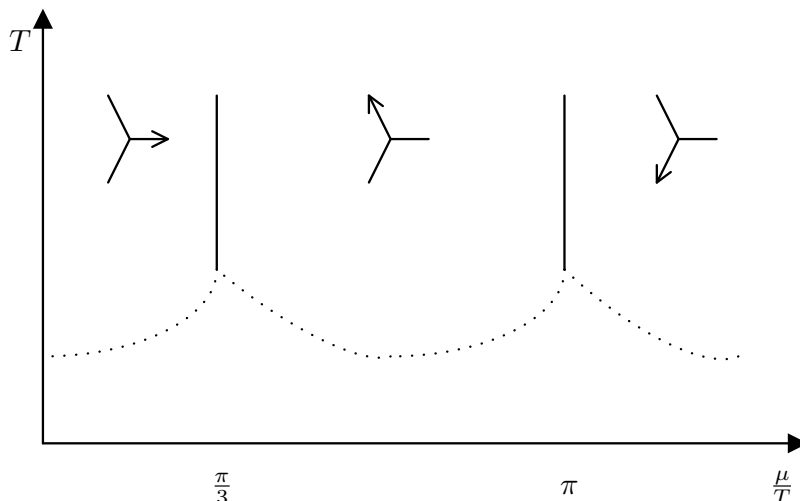


Figure 1. A Sketch of the phase diagram of R-W transition.

where $\gamma_{j=1,2,3} = i\gamma_j^E$ and $\gamma_4^E = \gamma_0$. The tangent space Wick rotation [55] also yields the same result.

Note that, the substitution $A_0^{\text{EM}} \rightarrow iA_4^{\text{EM}}$ corresponds to an imaginary electric field, or Euclidean electric field, which can also be viewed as an analytical extension.

On the other hand, the action with imaginary chemical potential can be written as

$$\mathcal{L}_q = \bar{\psi}_q \not{D}_\mu \psi_q + \bar{\psi}_q i \not{A} \psi_q - i\mu \bar{\psi}_q \gamma_0 \psi_q. \quad (2.3)$$

A simple observation is that the case of the presence of an external electric field can be viewed as a stacking of volumes with different imaginary chemical potentials $\mu = Q_q e E_z z$ extending the \mathbf{z} -axis. The Lagrangian in eq. (2.3) has been studied and an R-W transition is predicted and verified by lattice simulations. The definition feature of the R-W transition is the presence of imaginary part of the Polyakov loop. The sketch of the phase diagram of R-W transition is shown in figure 1. At high temperatures, there is a first order phase transition that the phase of the Polyakov loop is $2n\pi/3$, when $(2n - 1)\pi/3 < \mu/T < (2n + 1)\pi/3$, where n are integers. For the case of Euclidean electric field, some questions arise. Is there also R-W transition induced by an external uniform electric field? Is it appropriate to study the case of external electric field as a stacking of volumes with different imaginary chemical potentials? To answer those questions, the R-W phase induced by the external electric field is studied using the lattice approach.

By using the staggered fermion [56, 57], the action can be discretized as

$$S_G = \frac{\beta}{N_c} \sum_n \sum_{\mu > \nu} \text{Re tr} [1 - U_{\mu\nu}(n)], \quad (2.4)$$

$$S_q = \sum_n \left(\sum_{\mu} \sum_{\delta = \pm\mu} \bar{\chi}(n) U_\delta(n) V_\delta(n) \eta_\delta(n) \chi(n + \delta) + 2am \bar{\chi} \chi \right),$$

where a is the lattice spacing, S_G is the Wilson gauge action [57, 58] where $\beta = 2N_c/g_{\text{YM}}^2$ with g_{YM} the coupling strength of the gauge fields to the quarks, m is the fermion mass,

β	r_0/a	a^{-1} (MeV)	β	r_0/a	a^{-1} (MeV)
5.30	3.079(30)	1215(12)	5.48	4.906(46)	1936(18)
5.32	3.277(42)	1293(16)	5.50	5.189(36)	2048(14)
5.34	3.484(50)	1375(20)	5.52	5.435(60)	2145(24)
5.36	3.677(31)	1451(12)	5.54	5.579(51)	2202(20)
5.38	3.924(45)	1549(18)	5.56	5.829(31)	2300(12)
5.40	4.113(40)	1623(16)	5.58	6.133(47)	2420(19)
5.42	4.382(58)	1730(23)	5.60	6.386(46)	2520(18)
5.44	4.561(30)	1800(12)	5.62	6.545(39)	2583(15)
5.46	4.808(61)	1898(24)	5.64	6.957(55)	2746(22)

Table 1. The coupling constant β and the lattice spacing matched by using $r_0 = 0.5$ fb.

$U_\mu = e^{iaA_\mu}$, $V_\mu = e^{iaeA_\mu^{\text{EM}}}$, $\eta_\mu(n) = (-1)^{\sum_{\nu < \mu} n_\nu}$ and $U_{-\mu}(n) = U_\mu^\dagger(n - \mu)$, $V_{-\mu}(n) = V_\mu^*(n - \mu)$, $\eta_{-\mu} = -\eta_\mu(n - \mu)$. A twisted boundary condition is applied to ensure gauge invariance [46, 59–61], therefore we use

$$f = Q_q a^2 F = \frac{2k\pi}{L_\mu L_\nu}, \quad k \in \mathbb{Z}, \quad (2.5)$$

$$V_\nu = e^{ifn_\nu}, \quad V_\mu(n_\mu = L_\mu) = e^{-ifL_\mu n_\nu}.$$

where L_μ is the extent at direction μ .

In lattice simulations, the origin of the axis is set to be the middle of the spatial volume and at $n_\tau = 1$. With twisted boundary condition, S_q is U(1) gauge invariant, i.e. free of gauge choice (but different gauge choice will result in different twisted boundary conditions), and therefore the results do not depend on the gauge choice. For \mathbf{E} at the \mathbf{z} -direction and for axial gauge, $V_\mu(n) = 1$ except for

$$V_\tau(n) = e^{-iaQ_q e E_z z}, \quad V_z(a^{-1}z = L_z/2 - 1) = e^{iaQ_q e E_z L_z \tau}, \quad (2.6)$$

with quantized electric field $a^2 E_z = 6k\pi/L_\tau L_z$ so that f satisfies $2k\pi/L_\tau L_z$ with $|Q_q| = 1/3$. In the simulation, we use $L_x \times L_y \times L_z \times L_\tau = 12 \times 12 \times 12 \times 6$, therefore $a^{-1}z = -6, -5, \dots, 5$, $a^{-1}\tau = 0, 1, \dots, 5$ and $a^2 E_z = k \times \pi/12$. In this work, we use $k = 0, 1, \dots, 12$. The case of $k = 12 + n$ is equivalent as $k = 12 - n$ with an electric field on the opposite direction, where n are integers. Note that, for $a^2 e E_z \sim \mathcal{O}(1)$ or larger, the results suffer from strong discretization errors. In this case, the lattice action can no longer approximate the presence of external electric field well. Therefore, in sections. 3.2.3, 3.2.4 and 3.3.3 which are closely related to physical phenomena, we only consider the results with $0 \leq k \leq 4$.

3 Numerical results

3.1 Matching

The lattice simulation is performed with the help of **Bridge++** package [62]. To study the effect of external electric field, the simulation is carried out with $N_f = 1 + 1$, where

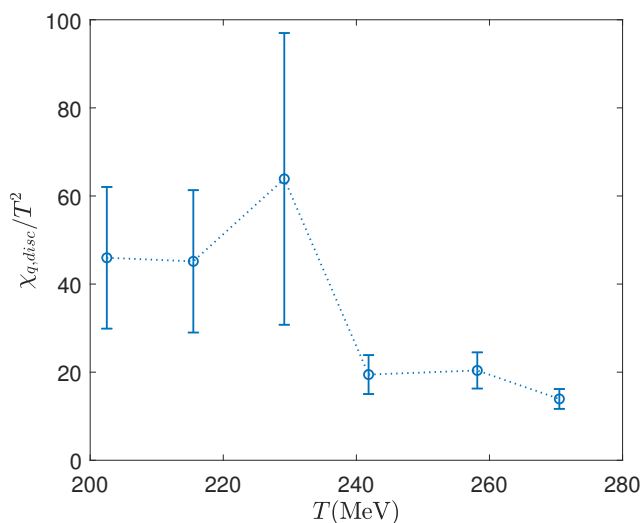


Figure 2. $\chi_{q,\text{disc}}/T^2$ as a function of T .

u and d quarks carrying different electric charges. The bare mass is chosen as $m_q = 0.1a^{-1}$ for both fermion fields where a is lattice spacing, when the electric field is not presented, the two fermion fields degenerate and $N_f = 2$. The coupling constant of gauge field β , and the corresponding a are listed in table 1. The lattice spacing is matched by measuring static quark potential $V(r)$ [63–65] and matching the ‘Sommer scale’ r_0 to $r_0 = 0.5$ fm [66–68] at low temperature (at $L_\tau = 48$). Throughout this paper, the statistical error is estimated as $\sigma = \sigma_{\text{jk}}\sqrt{2\tau_{\text{ind}}}$ [57], where σ_{jk} is statistical error calculated using ‘jackknife’ method, and $2\tau_{\text{ind}}$ is the separation of molecular dynamics time units (T.U.) such that the two configurations can be regarded as independent, which is calculated by using ‘autocorrelation’ with $S = 1.5$ [69] on the bare chiral condensation of quark (u quark in the case of $N_f = 1 + 1$). When matching, we use 200 trajectories as thermalization, and 1000 configurations are measured for each β . In the following, for each β , $200 + 3000 \times 13$ trajectories are simulated. The first 200 trajectories are discarded for thermalization, then 3000×13 trajectories are simulated with sequentially growing $a^2eE_z = k\pi/12$ for $k = 0, 1, 2, \dots, 12$. The first 100 trajectories of the 3000 are discarded for thermalization and 2900 configurations are measured for each β .

The pseudo critical temperature is determined at $E_z = 0$ by using disconnected susceptibility of chiral condensation defined as [70]

$$\chi_{q,\text{disc}} = \frac{N_f^2}{16L_x^3L_\tau} \left(\langle \text{tr} [D_q^{-1}]^2 \rangle - \langle \text{tr} [D_q^{-1}] \rangle^2 \right), \quad (3.1)$$

which is depicted in figure 2. It can be found that $\beta_c = 5.34$ and $T_c = 229$ MeV. Note that, for different β , m_q is different.

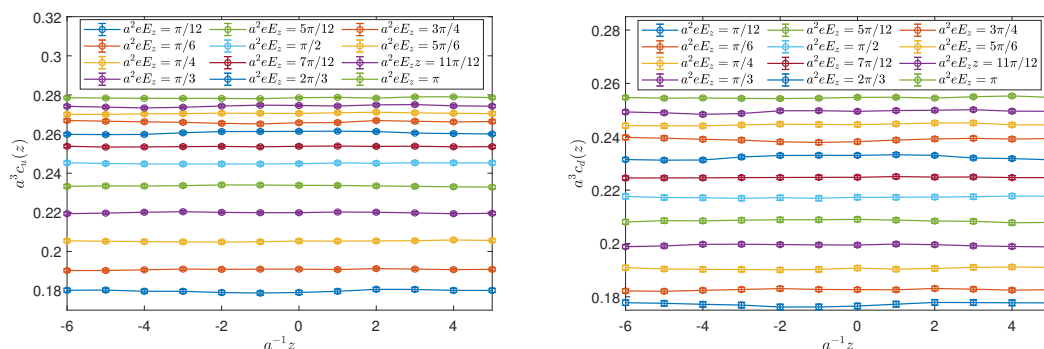


Figure 3. $c_u(z)$ (the left panel) and $c_d(z)$ (the right panel) at $\beta = 5.3$.

3.2 Chiral condensation

Since the bare mass m_q is different for different lattice spacing, we directly use $c_q = \langle \bar{\psi}_q \psi_q \rangle / V$ where V is volume. Such a definition has the problem of renormalization and is not suitable for comparison between different temperatures (there would have been difficulties to compare between different temperatures since m_q is different at different temperatures in our simulations), but can show the pattern of c_q with different E_z . Other quantities of interest are charge density defined as $c_q^4 = \langle \bar{\psi}_q \gamma_4 \psi_q \rangle / V$, and current density $c_q^3 = \langle \bar{\psi}_q \gamma_3 \psi_q \rangle / V$. In terms of staggered fermion field, they are

$$\begin{aligned}
 c_q &= \frac{1}{4L_x L_y L_z L_\tau} \frac{2}{a^3} \langle \sum_n \bar{\chi}(n) \chi(n) \rangle, \\
 c_q^\mu &= \frac{1}{4L_x L_y L_z L_\tau} \frac{1}{a^3} \langle \sum_n \eta_\mu(n) \sum_{\delta=\pm\mu} \bar{\chi}(n) U_\delta(n) V_\delta(n) \chi(n + \delta) \rangle.
 \end{aligned}
 \tag{3.2}$$

In order to study the influence of the chemical potential as the coordinate z changes, we also define $c_q(z)$, as $c_q(z) = \langle \sum_{n_z=z} \bar{\psi}_q(n) \psi_q(n) \rangle / (L_x L_y L_\tau)$, which is the chiral condensation of a z -slice. $c_q^{3,4}(z)$ are defined similarly. In the following, c_q and c_q^3 are treated as real numbers, and c_q^4 is treated as complex.

3.2.1 The Z distribution of chiral condensation

As introduced, one of our main concerns is whether the imaginary chemical potential, which varies with coordinate z , brings about a distribution that varies with z or whether it brings about an overall change. We find that the results depend on the temperature at which the quark matter is located. For $\beta = 5.3$ and $\beta = 5.64$, $c_q(z)$ are shown in figures 3 and 4. As can be seen, the chiral condensation rises as the electric field strength increases. The difference is that for lower temperatures, the chiral condensation does not appear to vary with the coordinate z . For high temperatures, it is clearly an oscillatory function of z . The shape of the function is consistent with a trigonometric function.

As a signature of whether the chiral condensation varies with z , we borrow the definition of standard deviation and define the magnitude of the oscillation of the chiral

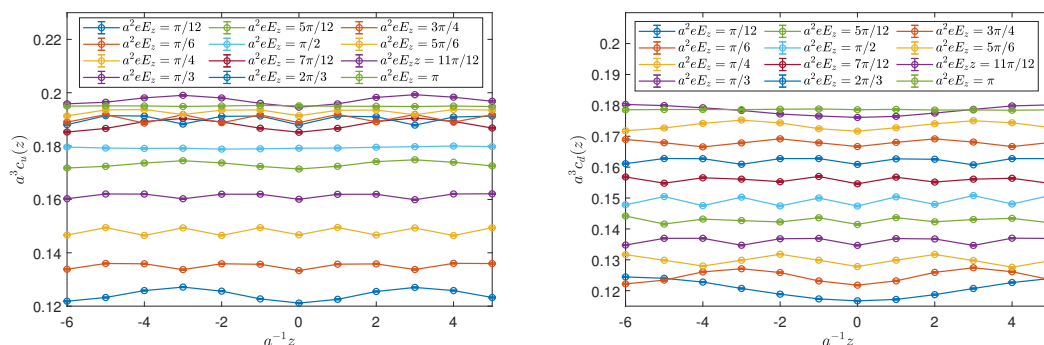


Figure 4. Same as figure 3 but for $\beta = 5.64$.

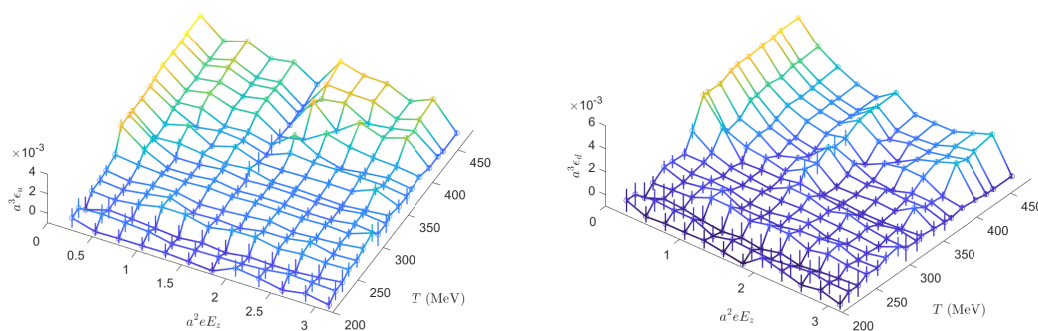


Figure 5. ϵ_u (the left panel) and ϵ_d (the right panel) as functions of temperature T and E_z .

condensation over z , as

$$\epsilon_q(T, E_z) = \sqrt{\frac{1}{L_z - 1} \sum_z \left(c_q^{T, E_z}(z) - \frac{1}{L_z} \sum_{z'} c_q^{T, E_z}(z') \right)^2}, \quad (3.3)$$

where $c_q^{T, E_z}(z)$ is $c_q(z)$ at temperature T and electric field strength E_z . When $E_z = 0$, there is no imaginary chemical potential that varies with z , therefore $\epsilon_q(T, 0)$ are set as baselines, and we define $\epsilon_q(T, E_z) = \epsilon_q(T, E_z) - \epsilon_q(T, 0)$. ϵ_q are shown in figure 5. Generally, the amplitude of oscillation grows with temperature. It can also be observed that, for the case of d quark whose electric charge is $-1/3$, the oscillation disappears at $a^2 e E_z = \pi$, for the case of u quark whose electric charge is $2/3$, the oscillation disappears at $a^2 e E_z = \pi/2$ and $a^2 e E_z = \pi$. This can be explained when the frequency of the oscillation is investigated.

Since the linearly changed imaginary chemical potential leads to a periodic change in the partition function, it can be speculated that the chiral condensation that oscillates periodically with the z -direction is a reflection of the linearly varying imaginary chemical potential. That is, at high temperatures, the whole system looks more inclined to be a simple combination of z -slices corresponding to different imaginary chemical potentials that reach equilibrium independently and then come together. This implies that the chiral

condensation located at a certain place does not feel the imaginary chemical potential far away perhaps due to some screening effect and the effect of imaginary chemical potential is therefore a short-range effect on the chiral condensation. On the contrary, when the oscillation disappears, the whole system must be considered as a whole, so that when equilibrium is reached, the chiral condensation located at a certain place can feel the overall distribution of the imaginary chemical potential, and the effect of imaginary chemical potential is therefore a long-range effect on the chiral condensation.

3.2.2 The fitting of chiral condensation

It has been shown, when oscillating, $c_q^{T,E_z}(z)$ is approximately a trigonometric function. We find that, $c_q^{T,E_z}(z)$ can be fitted as

$$c_q^{T,E_z}(z) = A_q^{T,E_z} + B_q^{T,E_z} \cos(af_c z Q_q e E_z), \quad (3.4)$$

where A_q^{T,E_z} can be viewed as an overall change of the chiral condensation, B_q^{T,E_z} is the amplitude of oscillation, f_c is the frequency of the oscillation.

$c_q^{T,E_z}(z)$ is fitted according to the ansatz in eq. (3.4) using the following steps.

1. For a fixed temperature (a fixed β), choose an initial value for f_c .
2. Find $A_q^{E_z}$ and $B_q^{E_z}$ which minimizes the error $\sum_z \delta^2(q, k, z)$ where $\delta(q, k, z) = A_q^{E_z^{(k)}} + B_q^{E_z^{(k)}} \cos(af_c z Q_q e E_z^{(k)}) - c_q^{E_z^{(k)}}(z)$, and $E_z^{(k)} = k\pi/12a^{-2}$.
3. For $A_q^{E_z}$ and $B_q^{E_z}$ obtained in step 2, find f_c which minimize the error $\sum_{q,k,z} \delta^2(q, k, z)$.
4. Repeat step 2 and 3 until f_c converges.
5. Apply step 2 for the last time and finish the fit.

The results of the fit depend on the initial value chosen for f_c , therefore, we fit the case of $a^2 E_z = \pi/12$ for u quark according to the ansatz in eq. (3.4) first to set the initial value for f_c . To ensure reliability, $c_u(z)$ at $a^2 e E_z = \pi/2$ and $a^2 e E_z = \pi$, $c_d(z)$ at $a^2 e E_z = \pi$ are excluded in the fit.

Taking the case of $\beta = 5.64$ for example, $c_q^{E_z}(z)$ and fitted $c_q^{E_z}(z)$ are shown in figures 6 and 7. Note that the dashed and solid lines are only shown for visual guidance, but not the images of $c_q(z)$. In this paper, we use $\chi^2/d.o.f.$ to estimate the goodness of fits, which is defined as

$$\chi^2/d.o.f. = \frac{1}{M - N} \sum_i^M \frac{(f(x_i, \vec{\alpha}) - y_i)^2}{\sigma_i^2}, \quad (3.5)$$

where M is the number of points (x_i, y_i) participated in the fit, $f(x_i, \vec{\alpha})$ is the result of fit with $\vec{\alpha} = (\alpha_1, \alpha_2, \dots, \alpha_N)$ representing the N fit parameters, σ_i is the statistical error for y_i .

To ensure reliability, we only fit $c_q(z)$ in the regions with strong oscillations. Starting from $\beta = 5.46$, c_q^{T,E_z} at $a^2 e E_z = \pi/12$ are one order of magnitude larger than the statistical errors of c_q^{T,E_z} . In the case $\beta \geq 5.46$, we find $\chi^2/d.o.f. = 0.48 \sim 1.07$ for different temperatures.

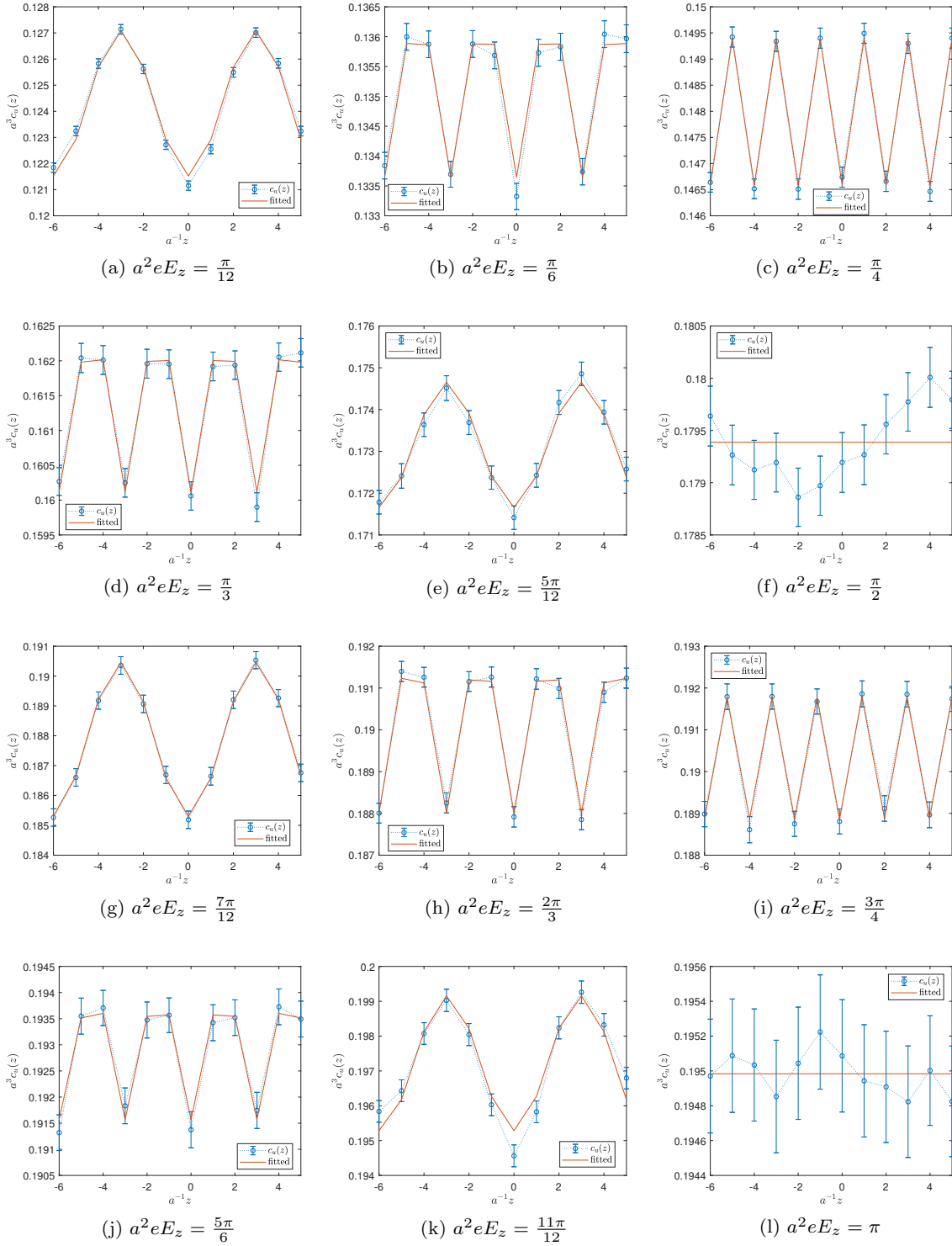


Figure 6. $c_u(z)$ at $\beta = 5.64$ compared with the results of fittings. Note that, the dashed and solid lines are only shown for visual guidance, but not the images of $c_u(z)$.

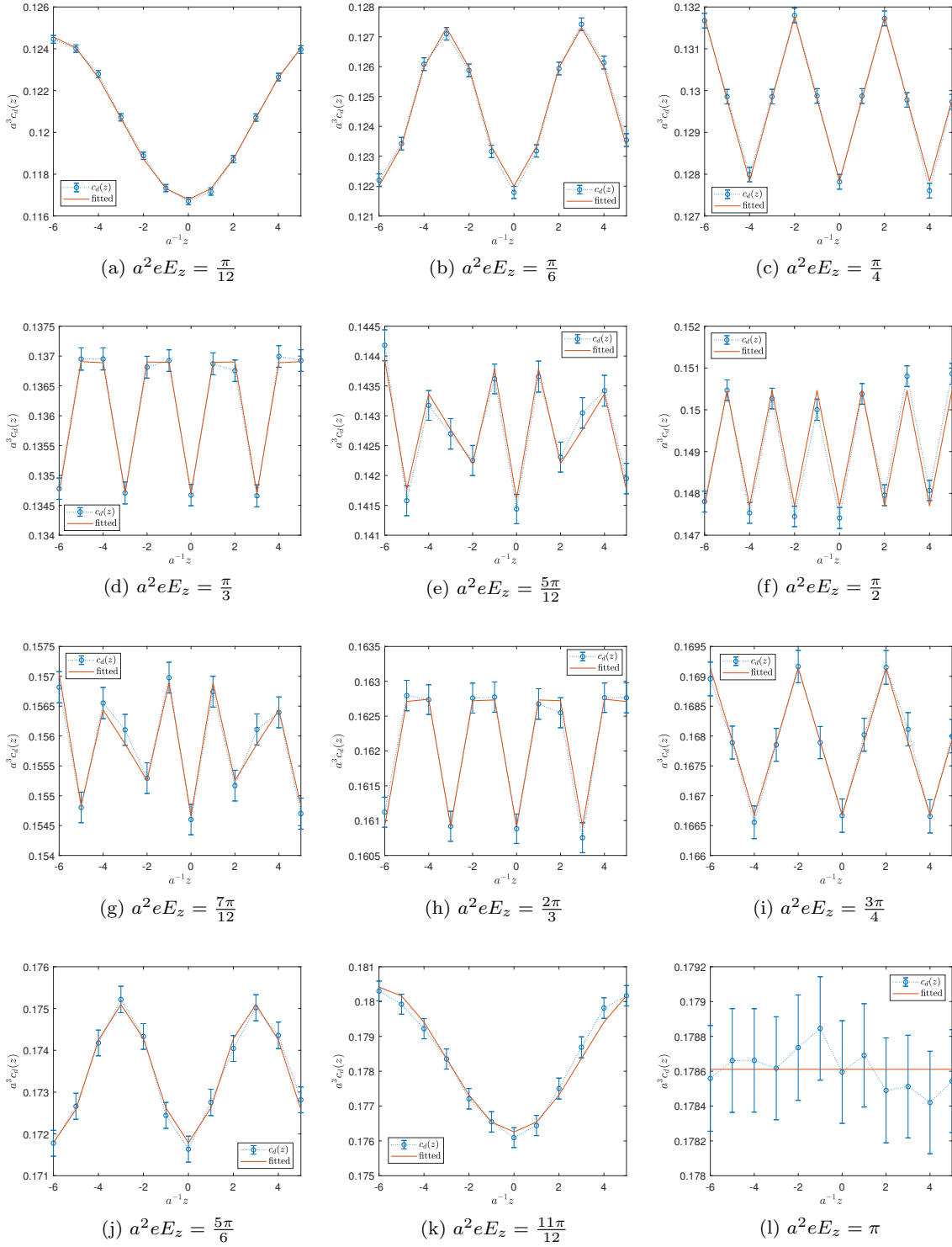


Figure 7. Same as figure 6 but for $c_d(z)$ at $\beta = 5.64$.

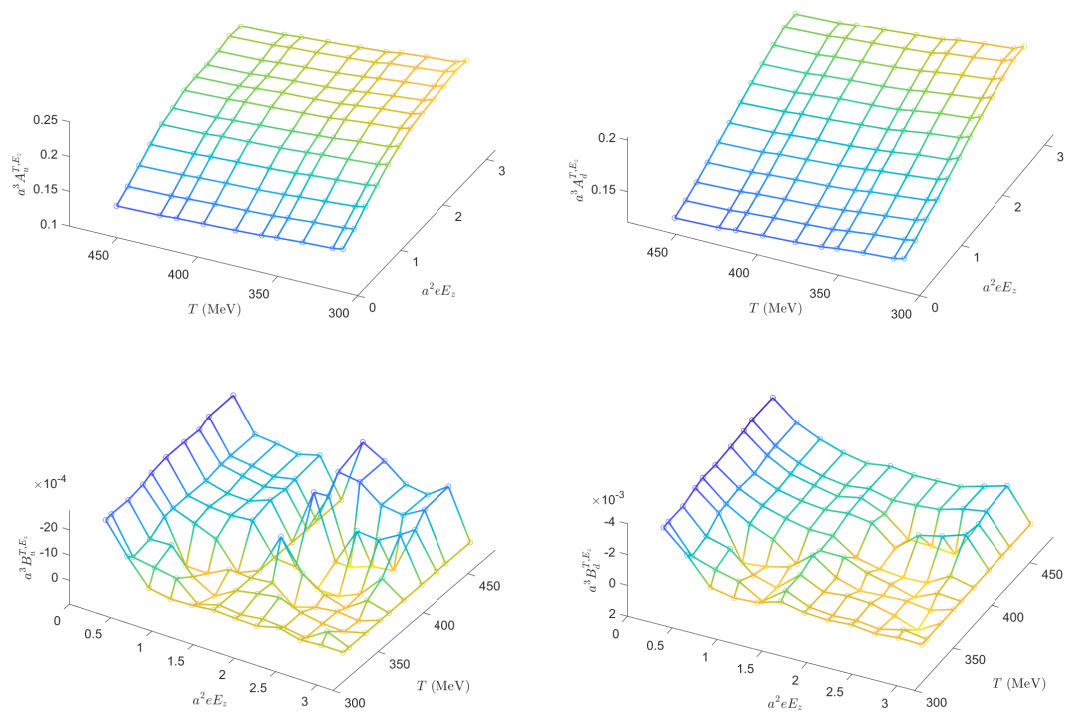


Figure 8. A_q and B_q as functions of temperature and E_z .

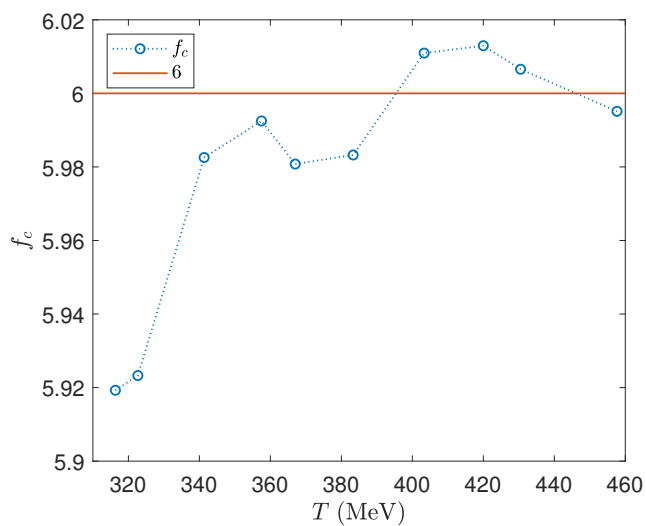


Figure 9. f_c as a function of temperature T .

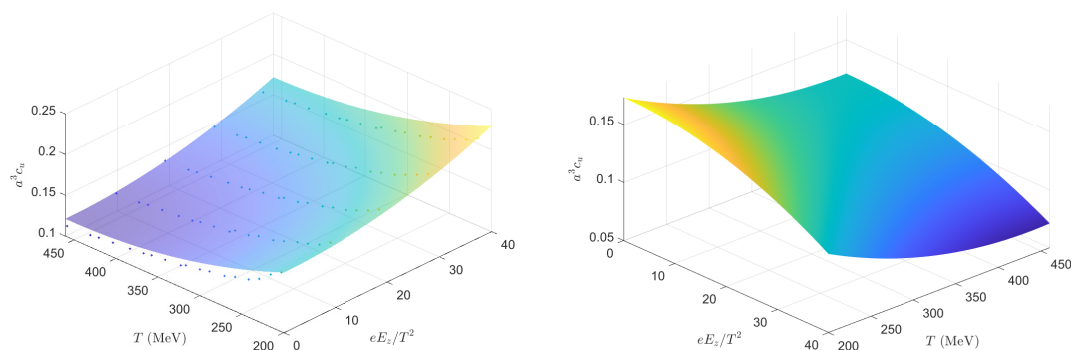


Figure 10. c_u^{T,E_z} and c_u^{T,E_z} fitted using eq. (3.6) (the left panel) and analytical extension of fitted c_u^{T,E_z} (the right panel).

A_q^{T,E_z} and B_q^{T,E_z} are shown in figure 8, f_c are shown in figure 9. It can be observed that, A_q grows with E_z and decrease with temperature. The overall effect of the electric field on the chiral condensation will be investigated later. Meanwhile, B_q is consistent with ϵ_q in figure 5. The amplitude of oscillation grows with the temperature and decreases with the electric field strength.

Another interesting and noteworthy conclusion is that $f_c \approx 6$ is a constant integer for different flavors at different temperatures and different electric field strengths. This also explained the phenomena that the oscillation disappears for $c_u(z)$ at $a^2 eE_z = \pi/2$ and $a^2 eE_z = \pi$, for $c_d(z)$ at $a^2 eE_z = \pi$. Since $a^2 f_c Q_u eE_z = 2\pi$ for $a^2 eE_z = \pi/2$ and 4π for $a^2 eE_z = \pi$, $a^2 f_c Q_d eE_z = -2\pi$ for $a^2 eE_z = \pi$.

The frequency f_c actually responds to the U(1) gauge field in eq. (2.6). When $k = 1$ and $f = 6\pi/(L_z L_\tau) = \pi/12$, the flux through the $z - \tau$ plane is 6π , and for quarks, the periods of oscillations along the z coordinate are exactly $Q_q \times 6\pi$. Thus, the frequency along z coordinate is actually $f_c = L_\tau = 6$.

It should be pointed out that, so far it is not able to exclude other cases, for example, f_c may not be L_τ , but $2N_c$, or $-2/Q_d$, as well as possibly $L_z/2$. It will be necessary to use other simulations to finally verify $f_c = L_\tau$. But we prefer f_c to be L_τ , and in the following, we use L_τ directly instead of f_c to denote the frequency.

3.2.3 The chiral condensation as a function of electric field strength

The relationship between chiral condensation and the electric field strength is one of the questions of interest in this work. When the system is considered as a whole, c_q as functions of T and E_z is calculated. The results suffer from strong discretization errors at large E_z , therefore only the results for $0 \leq a^2 eE_z \leq \pi/3$ are presented.

It needs to be kept in mind that the relationship between c_q and temperature is not simple, as the renormalization is not applied, it is affected by the relationship between c_q and lattice spacing a , in addition, as am_q is a constant, it is also messed up by the relationship between c_q and m_q at the same time. Apart from those, the electric field

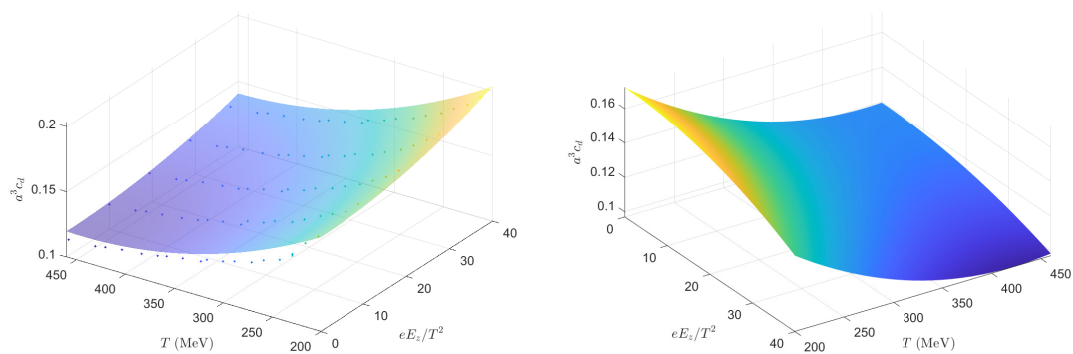


Figure 11. Same as figure 10 but for c_d^{T, E_z} .

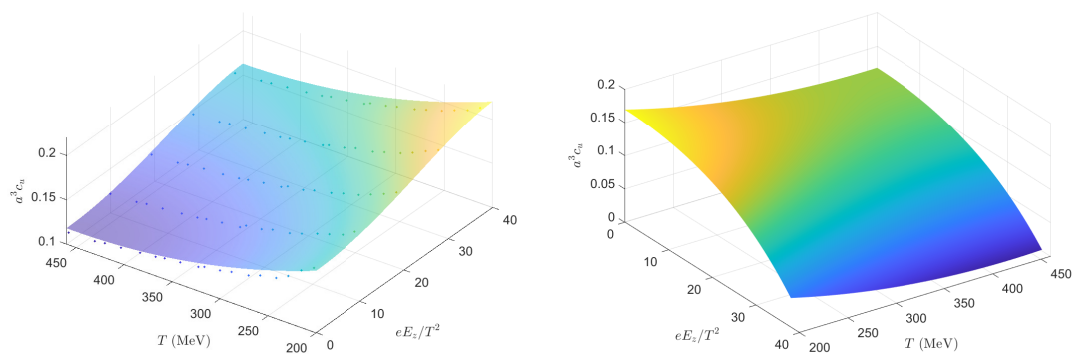


Figure 12. Same as figure 10 but fitted using eq. (3.7).

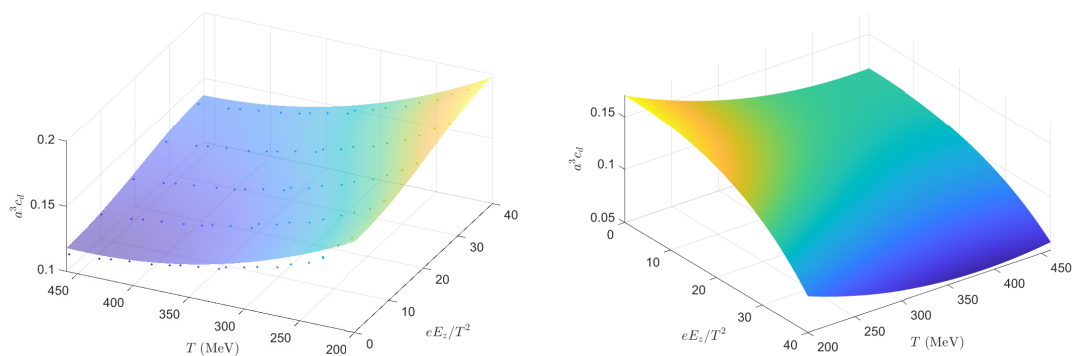


Figure 13. Same as figure 11 but fitted using eq. (3.7).

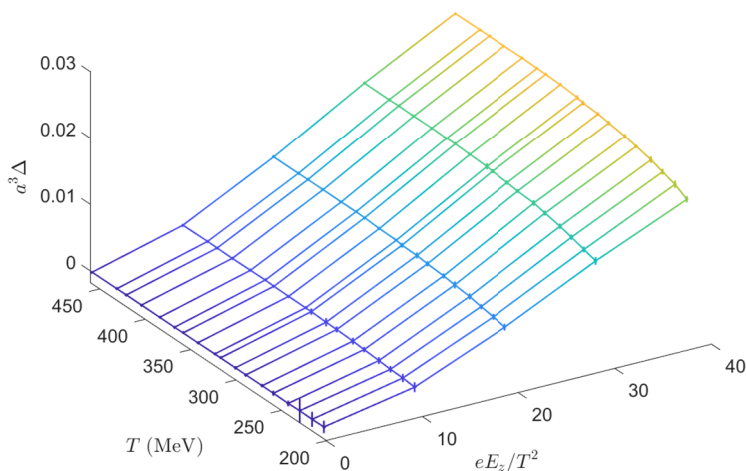


Figure 14. $\Delta = c_u - c_d$ as a function of T and eE_z/T^2 .

in physical units are different for different a , therefore in this subsection, the results are present as functions of eE_z/T^2 instead of $a^2 eE_z$.

Although further verification is needed, it is useful to assume that chiral condensation is still perturbable as the electric field strength varies. In other words, we assume $c_q^{T,E_z} \approx a_0(T) + a_1(T)E_z^2 + a_2(T)E_z^4 + \dots$. With this assumption, analytical extension can be applied to obtain the relationship between the chiral condensation and the real electric field strength. The ansatz of c_q^{T,E_z} up to the order of E_z^2 and E_z^4 are

$$c_q^{T,E_z} = (a_0 + a_1 T + a_2 T^2) + (b_0 + b_1 T) E_z^2, \quad (3.6)$$

$$c_q^{T,E_z} = (a_0 + a_1 T + a_2 T^2) + (b_0 + b_1 T) E_z^2 + (c_0 + c_1 T) E_z^4. \quad (3.7)$$

The results of c_u and c_d keeping up to E_z^2 are shown in the left panels of figures 10 and 11, respectively. The results of c_u and c_d keeping up to E_z^4 are shown in the left panels of figures 12 and 13, respectively. The $\chi^2/d.o.f.$ are 7.3 and 3.2 for c_u and c_d keeping up to E_z^2 , 2.5 and 1.9 for c_u and c_d keeping up to E_z^4 . In our simulation, we use an imaginary electric field strength. To obtain the relationship between c_q and E_z , an analytical extension is applied to rotate the electric field strength back to the real axis. The results of c_u and c_d keeping up to E_z^2 after analytical extension are shown in the right panels of figures 10 and 11, respectively. The results of c_u and c_d keeping up to E_z^4 after analytical extension are shown in the right panels of figures 12 and 13, respectively. Both the ansatz in eqs. (3.6) and (3.7) support the conclusion that the external electric field restores the chiral symmetry as predicted by previous works.

Moreover, since $|Q_u| > |Q_d|$, the effect of the electric field is larger for c_u than c_d . The difference defined as $\Delta = c_u - c_d$ (Δ is also $\langle \bar{\psi} \tau_3 \psi \rangle$ where τ_3 is the Pauli matrix) is also calculated and depicted in figure 14. It can be seen that, $a^3 \Delta$ is insensitive to temperature.

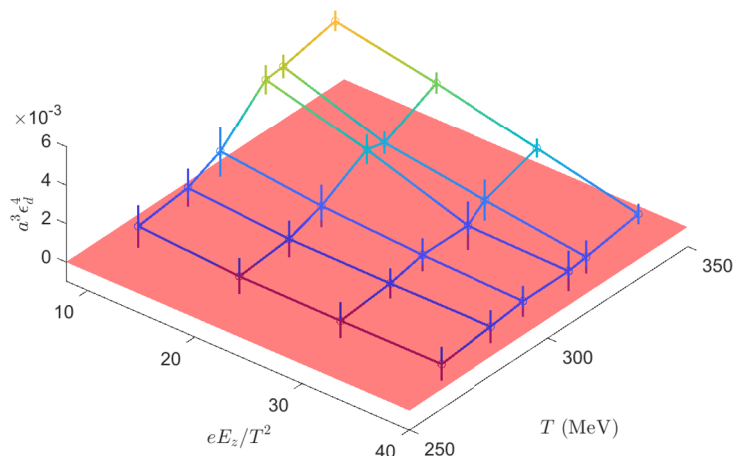


Figure 15. ϵ_d^4 as a function of temperature T and eE_z/T^2 .

3.2.4 The charge distribution

It has been pointed out that, in equilibrium, the electric and diffusion forces acting on quarks balance each other, which happens when there is a non-constant charge distribution [50, 51]. The charge density can be defined as $Q_q e \bar{q} \gamma_0 q$, which can be related with c_q^A defined in eq. (3.2). We find that, at high temperatures, the imaginary of c_q^A shows nontrivial dependence on z . As will be explained later, we concentrate on $\text{Im}[c_d^4]$. To show the oscillation of $\text{Im}[c_d^4]$, $\epsilon_d^4(T, E_z)$ is defined as same as $\epsilon_q(T, E_z)$ but with c_q^{T, E_z} replaced by $\text{Im}[c_d^4]$. ϵ_d^4 is shown in figure 15. Starting from $T \approx 300$ MeV, the imaginary of c_q^A starts to oscillate over z coordinate for $\pi/12 \leq a^2 e E_z \leq \pi/3$.

We find that, the frequencies of the oscillation are as same as those of $c_q(z)$, i.e., the $\text{Im}[c_q^{A, T, E_z}]$ can be fitted with the ansatz,

$$\text{Im} \left[c_q^{A, T, E_z}(z) \right] = A_q^{A, T, E_z} \sin(a L_\tau z Q_q e E_z). \quad (3.8)$$

For $\beta = 5.64$, $\text{Im} \left[c_q^4(z) \right]$ are shown in figure 16. $\chi^2/d.o.f.$ are found to be $0.086 \sim 0.118$. For c_u^4 , the case of $a^2 e E_z = \pi/4$ corresponds to no oscillation, that is the reason why ϵ_d^4 is used to show the oscillation. In all cases, $A_q^4 < 0$. We also find that $|A_d^4|$ decrease with E_z .

Another interesting quantity is c_q^3 . We find that, at high temperatures and at large E_z ($a^2 e E_z = \pi/3$), $c_u^3(z)$ also oscillates over z ($c_d^3(z)$ starts to oscillate at a larger E_z beyond our scope due the large discretization errors). To verify that the oscillations of $c_u^3(z)$ along z are not caused by not reaching the equilibrium, for $\beta = 5.64$ and $a^2 e E_z = \pi/3$, additional 6000 trajectories are simulated starting from $T.U. = 3000$. The results are shown in figure 17. Although $c_u^3(z)$ has a none trivial distribution, $c_u^3 = 0$. The none trivial $c_u^3(z)$ may indicate a none trivial meson condensation caused by Schwinger mechanism [41]. Also, since the case of a large E_z is affected by large discretization errors, it is possible that this is a fake phenomenon from discretization errors.

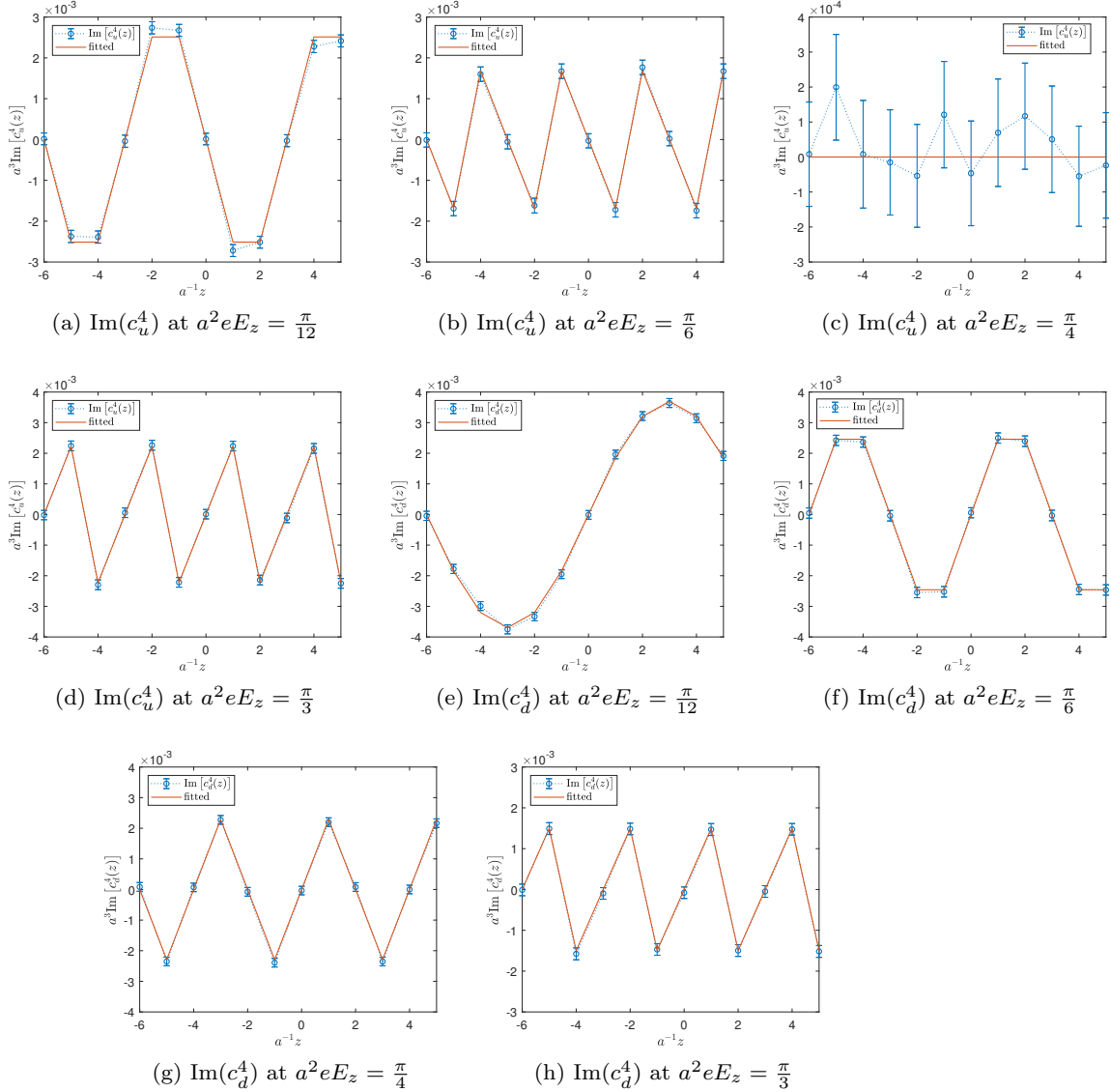


Figure 16. Same as figure 6 but for $\text{Im}[c_q^4(z)]$ at $\beta = 5.64$.

3.3 Polyakov loop

The signal of R-W transition can be observed by the phase of Polyakov loop, the latter is defined as

$$P(\mathbf{n}) = \prod_{n_\tau} U_\tau(\mathbf{n}, n_\tau), \quad P(z) = \frac{1}{L_x L_y} \sum_{n_x, n_y} P(\mathbf{n} = (n_x, n_y, a^{-1}z)), \quad P = \frac{1}{L_z} \sum_z P(z), \quad (3.9)$$

where the product in the definition of $P(\mathbf{n})$ is performed sequentially from $n_\tau = 0$ to $n_\tau = L_\tau - 1$, and $P(z)$ is an average of $P(\mathbf{n})$ over a z -slice, P is an average of $P(\mathbf{n})$ over the whole spatial volume.

For different β and $a^2 e E_z$, $|\langle P \rangle|$ and $\arg(\langle P \rangle)$ are shown in figure 18. The R-W transition is clearly presented according to the non-zero $\arg(\langle P \rangle)$ at lower temperatures.

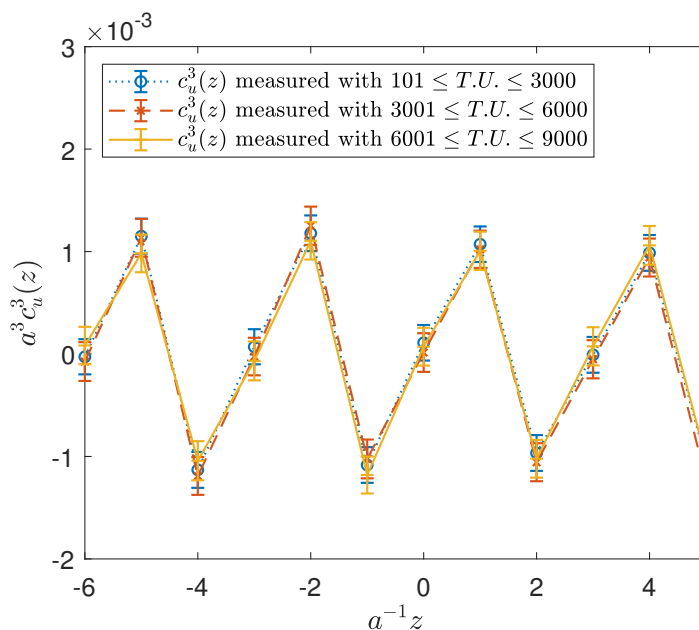


Figure 17. The oscillations of $c_u^3(z)$ along z measured using different configurations.

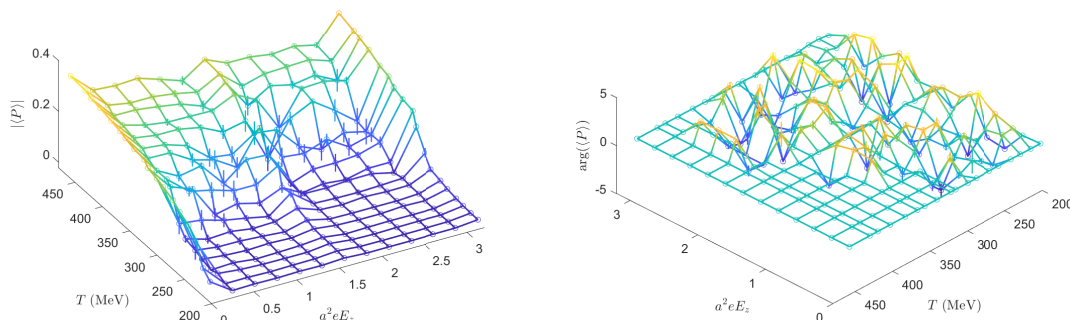


Figure 18. $|\langle P \rangle|$ (the left panel) and $\arg(\langle P \rangle)$ (the right panel) as functions of T and E_z .

3.3.1 The properties of Polyakov loop

The phase of the Polyakov loop is important to study the R-W transition. It is observed that the phase of the Polyakov loop is also oscillating with z , but quite different from the case of chiral condensation, the phase of Polyakov loop is oscillating at lower temperatures. Since a large E_z corresponds to a high frequency of oscillation and is not suitable for presentation, we show $P(z)$ only for $a^2 e E_z = \pi/12$, in the complex plane, similar to ref. [54]. The case of $\beta = 5.30$ and $\beta = 5.64$ are shown in figure 19, $\langle P(z) \rangle$ in the complex plane exhibits the shape of a pointed triangle for both low temperature and high temperature.

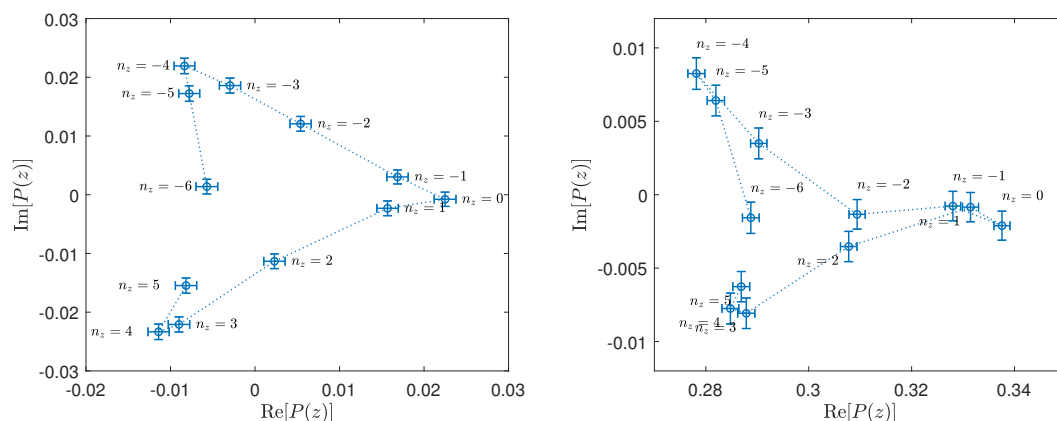


Figure 19. $\langle P(z) \rangle$ at $a^2 e E_z = \pi/12$ shown in the complex plane for $\beta = 5.3$ (the left panel) and $\beta = 5.64$ (the right panel).

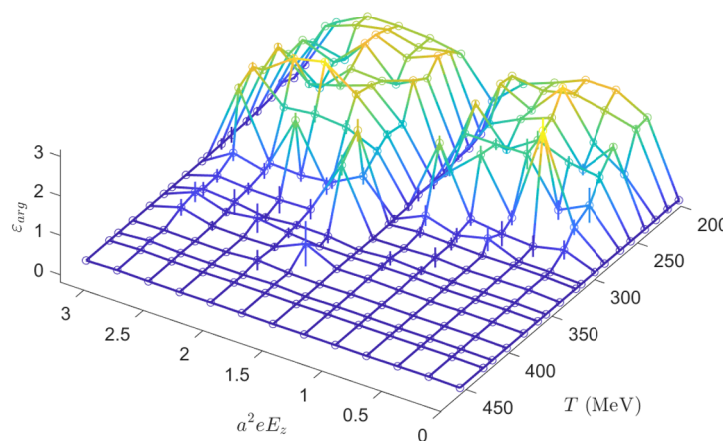


Figure 20. ε_{arg} as a function of T and E_z .

Similar as ε_q in eq. (3.3), we define

$$\varepsilon_{arg}(T, E_z) = \sqrt{\frac{1}{L_z - 1} \sum_z \left(\arg(\langle P^{T, E_z}(z) \rangle) - \frac{1}{L_z} \sum_{z'} \arg(\langle P^{T, E_z}(z') \rangle) \right)^2}. \quad (3.10)$$

ε_{arg} is shown in figure 20. Note that, for high temperatures, there are cases that $\arg(\langle P \rangle)$ is large while ε_{arg} is small. For $a^2 e E_z = \pi/2$, ε_{arg} is small. Those properties will be explained later.

For a lower temperature and a small external electric field, the phase of the Polyakov loop is consistent with the R-W transition. The cases of $\beta = 5.3$ and $\beta = 5.38$ at $a^2 e E_z = \pi/12$ are shown in figure 21. It can be seen that there are plateaus in the $\arg(\langle P(z) \rangle)$ located at $2n\pi/3$ where n are integers.

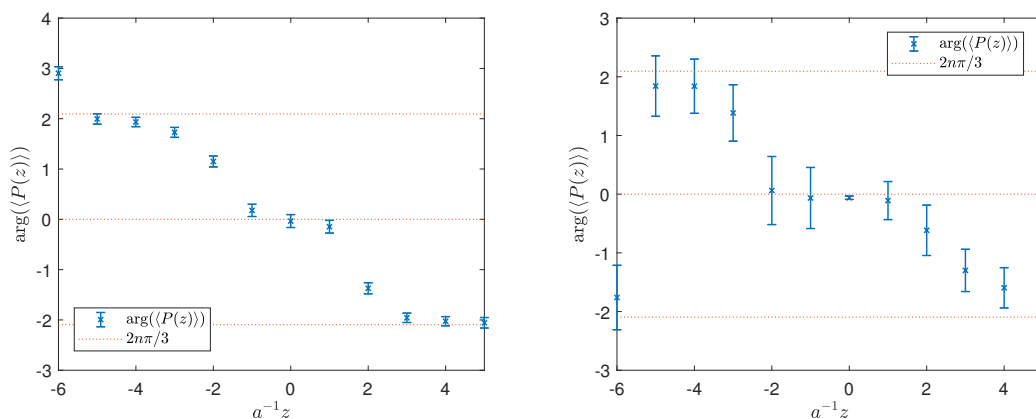


Figure 21. $\arg(\langle P(z) \rangle)$ at $a^2 e E_z = \pi/12$ for $\beta = 5.3$ (the left panel) and $\beta = 5.38$ (the right panel).

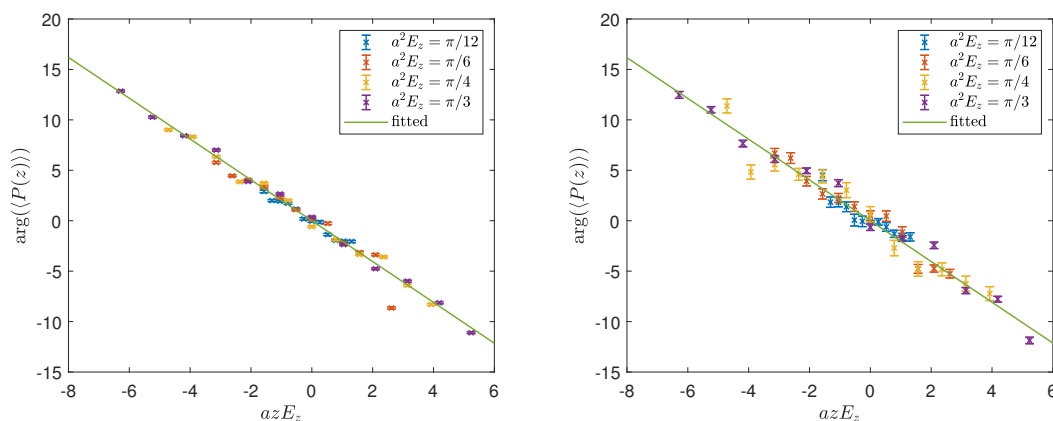


Figure 22. $\arg(\langle P(z) \rangle)$ and fitted $\arg(\langle P(z) \rangle)$ according to the ansatz in eq. (3.11) for $\beta = 5.3$ (the left panel) and $\beta = 5.38$ (the right panel).

Since $a^2 e \Delta E_z = \pi/12$ is large, the widths of the plateaus are narrow. For larger $a^2 e E_z$, the widths of plateaus can be neglected, and $\arg(\langle P(z) \rangle)$ tends to be a linear function of $z E_z$, therefore we assume

$$\arg(\langle P(z) \rangle) = a f_{\text{arg}} z e E_z. \quad (3.11)$$

By adding integer times of 2π , $\arg(\langle P(z) \rangle)$ is fitted according to eq. (3.11). The results of the fit depend on the manually added $2n\pi$ where n are integers, and to minimize the effect of the manually added $2n\pi$, we fit only for the case of $a^2 e E_z \leq \pi/3$. Taking $\beta = 5.3$ and $\beta = 5.38$ as examples, $\arg(\langle P(z) \rangle)$ and fitted $\arg(\langle P(z) \rangle)$ are shown in figure 22.

In the region $5.3 \leq \beta \leq 5.38$, $\arg(\langle P(z) \rangle)$ are fitted, and f_{arg} is shown in figure 23. The $\chi^2/d.o.f. = 6.54 \sim 42.7$ for different β , the worst case is $\beta = 5.3$. We find that $f_{\text{arg}} \approx -2$ which is a constant integer for different temperatures. This integer also explains

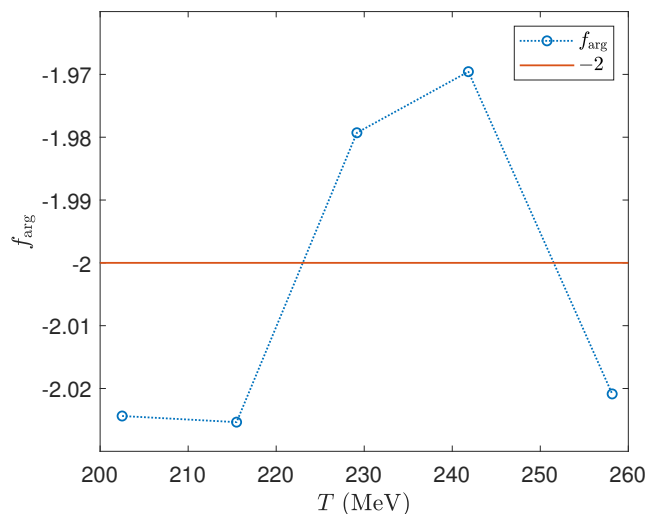


Figure 23. f_{arg} in eq. (3.11) as a function of temperature.

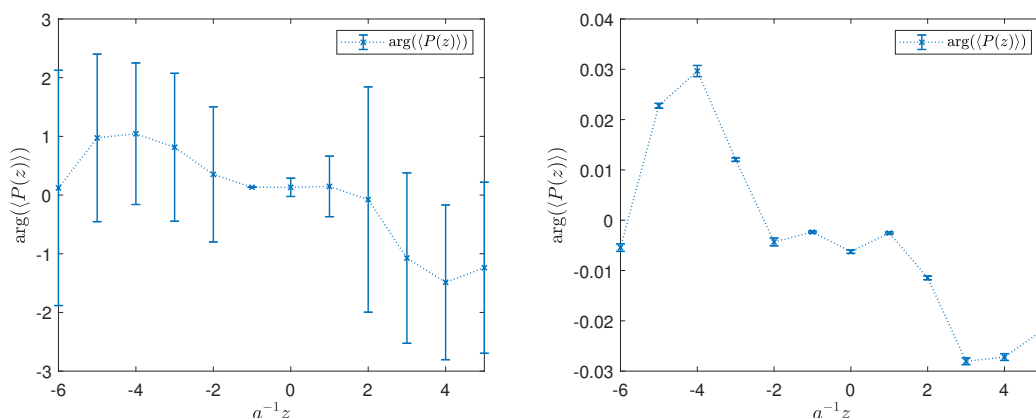


Figure 24. Same as figure 21 but for $\beta = 5.4$ (the left panel) and $\beta = 5.64$ (the right panel).

the phenomena $\arg(\langle P(z) \rangle) = 0$ and $\varepsilon_{\text{arg}} = 0$ for $a^2 e E_z = \pi$. However, the case of $a^2 e E_z = \pi/2$ cannot be explained, and will be postponed to section. 3.3.2.

Such behavior fits when $\beta < 5.4$. Starting from $\beta = 5.4$, the behavior of the phase of Polyakov loop becomes different. As examples, $\arg(\langle P(z) \rangle)$ at $\beta = 5.4$ and $\beta = 5.64$ and at $a^2 e E_z = \pi/12$ are shown in figure 24. It can be seen that, the variation of $\arg(\langle P(z) \rangle)$ is much smaller than the case in figure 21.

On the other hand, with growing temperatures the pattern of the $|\langle P(z) \rangle|$ gradually starts to become clear. Similar as ϵ_q , we define

$$\varepsilon_{\text{abs}}(T, E_z) = \sqrt{\frac{1}{L_z - 1} \sum_z \left(|\langle P^{T, E_z}(z) \rangle| - \frac{1}{L_z} \sum_{z'} |\langle P^{T, E_z}(z') \rangle| \right)^2}, \quad (3.12)$$

and $\epsilon_{\text{abs}}(T, E_z) = \varepsilon_{\text{abs}}(T, E_z) - \varepsilon_{\text{abs}}(T, E_z = 0)$. ϵ_{abs} is shown in figure 25.

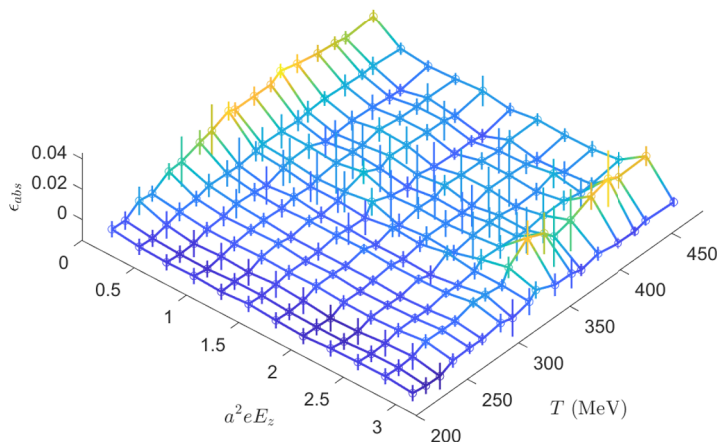


Figure 25. ϵ_{abs} as a function of T and E_z .

For $|\langle P(z) \rangle|$, we use the ansatz

$$|\langle P(z) \rangle| = A_{\text{abs}} + B_{\text{abs}} \cos(a f_{\text{abs}} z e E_z). \quad (3.13)$$

Using the method to fit for the chiral condensation, and using eq. (3.13), $|\langle P(z) \rangle|$ is fitted. As an example, the case for $\beta = 5.64$ is shown in figure 26, the $\chi^2/d.o.f. = 0.73$. It can be seen that, except for the cases $a^2 e E_z = 5\pi/12$ and $a^2 e E_z = 7\pi/12$, eq. (3.13) roughly describes the pattern of $|\langle P(z) \rangle|$. Similar as the case of chiral condensation, the range of $5.46 \leq \beta \leq 5.64$ is considered, and f_{abs} is shown in figure 27. Again, we find $f_{\text{abs}} \approx 2$ which is a constant integer.

At smaller E_z , another noteworthy interesting phenomenon is that $\epsilon_{u,d}$ in figure 5, ϵ_d^4 in figure 15 and ϵ_{abc} in figure 25 decrease with E_z in the small E_z region. This behavior implies that, the oscillation suddenly appears at a small non-zero E_z . It has been pointed out in refs. [50, 51] that, physical observables exhibit a discontinuity between $E = 0$ and any small $E > 0$. Our results can be seen as a support for the above conclusion.

3.3.2 An ansatz for the Polyakov loop

After combining the analysis of the phase of Polyakov and the absolute value of Polyakov loop, we conclude that Polyakov loop is consistent with ansatz

$$\langle P(z) \rangle = A_p + \sum_{q=u,d} C_q \exp(L_\tau Q_q i a z e E_z), \quad (3.14)$$

where C_q are real numbers (and $C_d > 0$, $C_u \geq 0$ after fit) and A_p is a complex number because there are cases that $\arg(\langle P \rangle)$ is large but ϵ_{arg} is small which corresponds to a complex A_p and $|A_p| \gg C_q$.

The ansatz in eq. (3.14) counts both the effect from u and d quarks, and is able to describe the following phenomena.

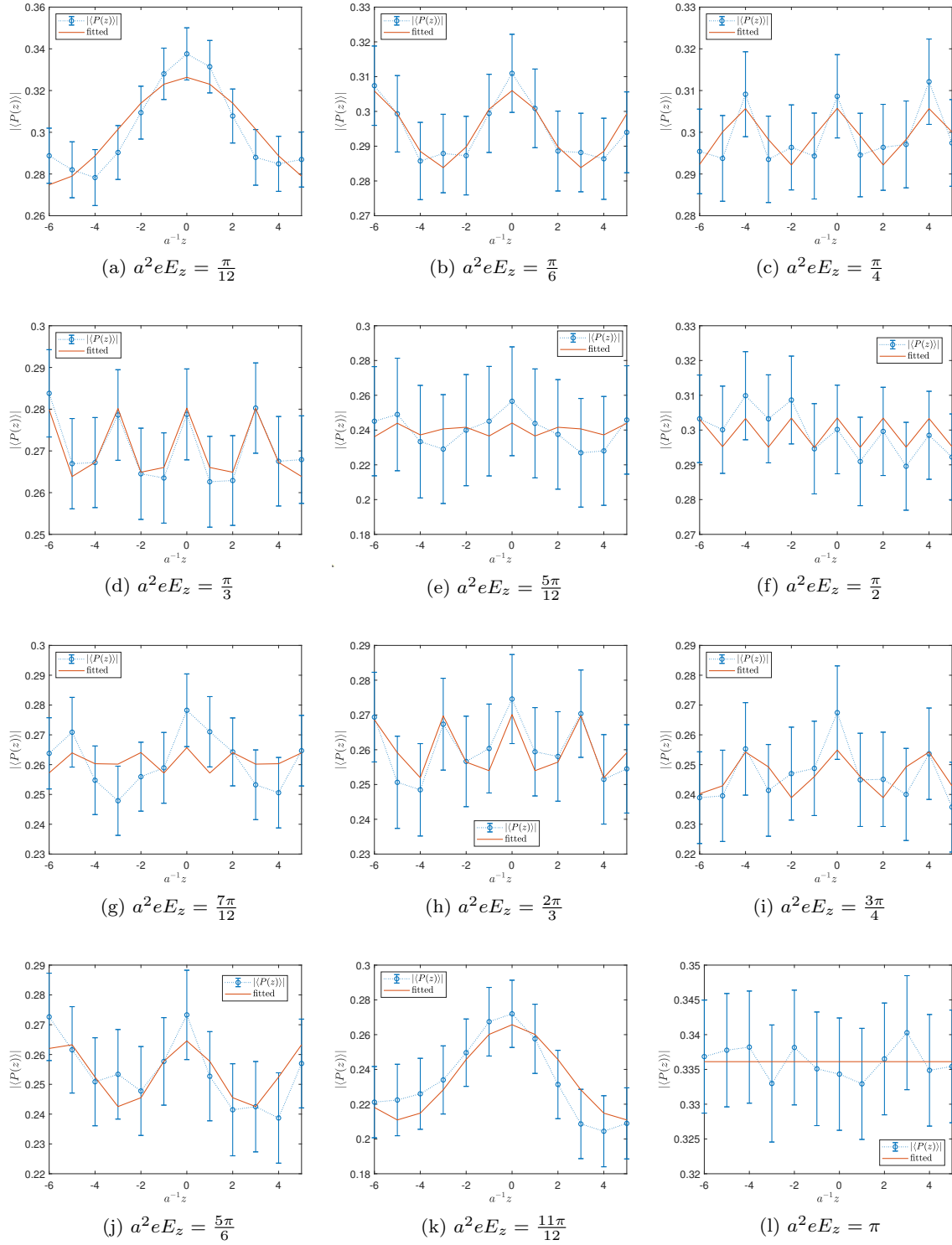


Figure 26. Same as figure 6 but for $|P(z)|$ at $\beta = 5.64$.

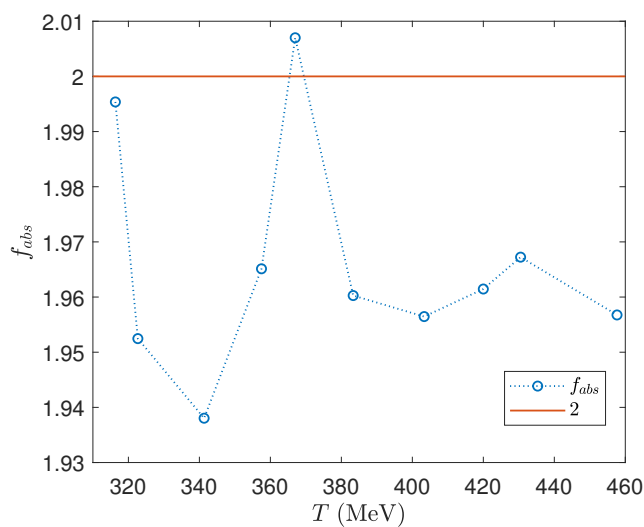


Figure 27. f_{abs} as a function of temperature.

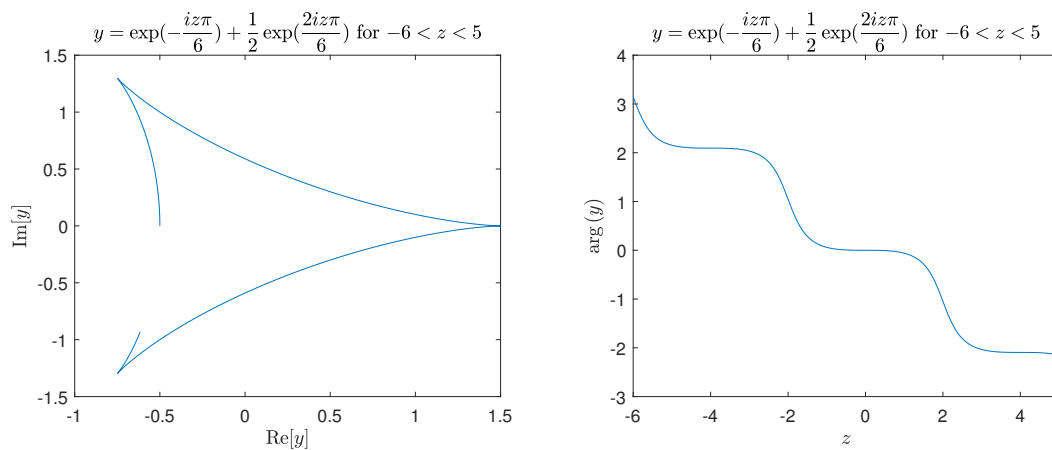


Figure 28. An example when $|A_p| \ll C_q$ and $C_u < C_d$, the $\langle P(z) \rangle$ in ansatz eq. (3.14) depicted in the complex plane (the left panel) and $\arg(P(z))$ (the right panel).

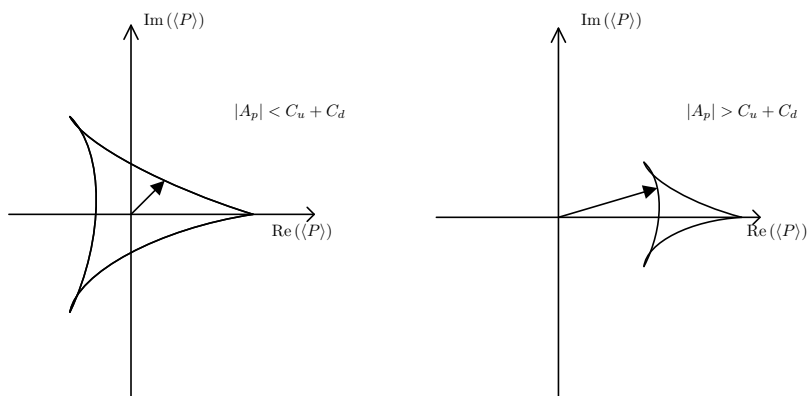


Figure 29. The difference patterns of the phase of the Polyakov loop when $|A_p| < C_u + C_d$ (the left panel) and $|A_p| > C_u + C_d$ (the right panel).

- As shown in the left panel of figure 28, for $|A_p| \ll C_q$ and $C_u < C_d$ the ansatz describes $\langle P(z) \rangle$ in the complex plane in the left panel of figure 19. Similarly, when $|A_p| \gg C_q$, the ansatz describes the right panel of figure 19.
- As shown in the right panel of figure 28, for $|A_p| \ll C_q$ and $C_u < C_d$, eq. (3.14) describes the phenomena in figure 21. With $C_d > C_u$, the effect of C_u term becomes small plateaus. Ignoring the plateaus, $f_{\text{arg}} = L_\tau \times Q_d = -2$, which explains the phenomena in figures 22 and 23.
- As shown in figure 29, when $|A_p| > C_q$, the phase of the Polyakov loop ranges in $[-\pi, \pi)$, when $|A_p| < C_q$, the phase of the Polyakov loop ranges in $(-\pi/2, \pi/2)$. With the growth of temperature, $|A_p| > C_q$, the phase of Polyakov loop when $\beta \geq 5.4$ in figure 24 can be explained.
- When $|A_p| \gg C_q$ and $C_u \ll C_d$, eq. (3.14) describes the oscillation in figure 26 and $f_{\text{abs}} = |L_\tau \times Q_d| = 2$ in figure 27 can be understood. A C_u term also explains the discrepancy of the ansatz in eq. (3.13) at $a^2 e E_z = 5\pi/12$ and $a^2 e E_z = 7\pi/12$.
- Apart from that, eq. (3.14) also explains the reason that ε_{arg} is small and $\arg(\langle P \rangle) \approx 0$ at $a^2 e E_z = \pi/2$. This can be attributed to a real A_p which is larger than $C_u + C_d$.

For $\beta = 5.3 \sim 5.64$, the $\langle P(z) \rangle$ are fitted, and we find $\chi^2/d.o.f. = 0.10 \sim 1.88$. To compare with the ansatz in eqs. (3.11) and (3.13), using eq. (3.14), $\chi^2/d.o.f. = 0.67 \sim 1.88$ for $\beta = 5.3 \sim 5.38$, and $\chi^2/d.o.f. = 0.24$ for $\beta = 5.64$. Taking the case of $\beta = 5.42$ which lies in the middle of the region $5.4 \leq \beta \leq 5.44$ as an example ($\chi^2/d.o.f. = 0.47$), the results are shown in figures 30 and 31. Eq. (3.14) is able to describe the pattern of $\langle P(z) \rangle$.

3.3.3 A criterion to distinguish the different behaviors of the Polyakov loop

In previous works, the susceptibility of the imaginary of the Polyakov loop is used to find out the phase diagram of the R-W transition. However, in our study, we did not see a clear signal of phase transition in this approach. This can be understood because from the point of view of the R-W phase transition, the phase transition point is about $\mu/T = \pi/3$ which is $a\mu = \pi/(3L_t) = \pi/18$. For our study, $a^2 \Delta e E_z = \pi/12$, so the case of the smallest electric field is already in the R-W phase. In terms of the chiral phase transition due to the strong electric field, the phase transition point is about $(500 \text{ MeV})^2$ magnitude in the previous study [36]. For the case of the smallest lattice spacing, which is $\beta = 5.3$, $\Delta e E_z \approx (621.5 \text{ MeV})^2$, and the case of the smallest electric field is already in chiral symmetry restored phase.

On the other hand, comparing the chiral condensation at high and low temperatures, or the behavior of Polyakov loop, we can find clear differences. At high temperatures, the chiral condensation and charge density oscillate with z coordinate. Another very clear difference is that if the ansatz in eq. (3.14) is correct, then the size relationship between $|A_p|$ and C_q causes a significant difference in Polyakov loop phase behavior as shown in figure 29.

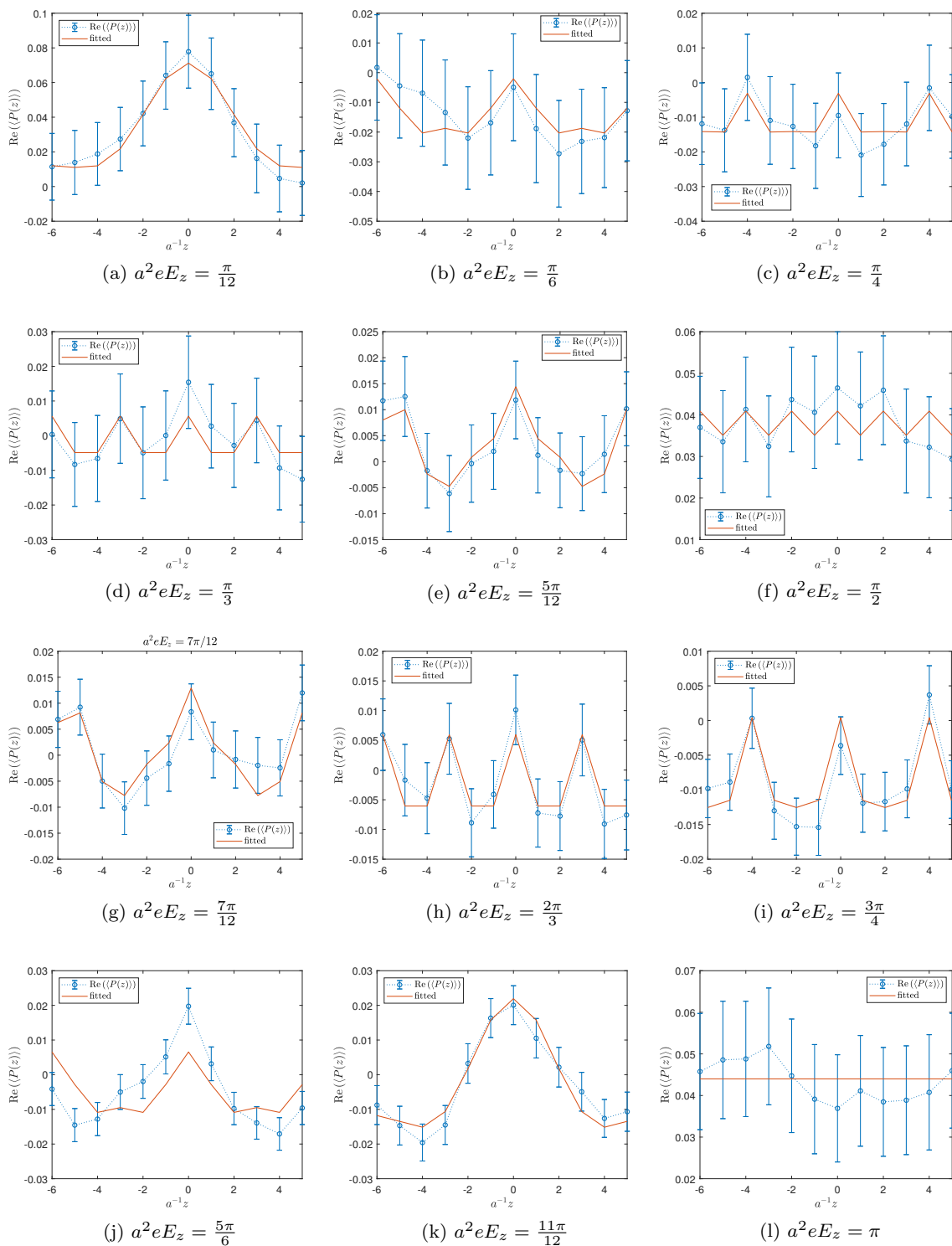


Figure 30. Same as figure 6 but for $\text{Re}(\langle P(z) \rangle)$ at $\beta = 5.42$.

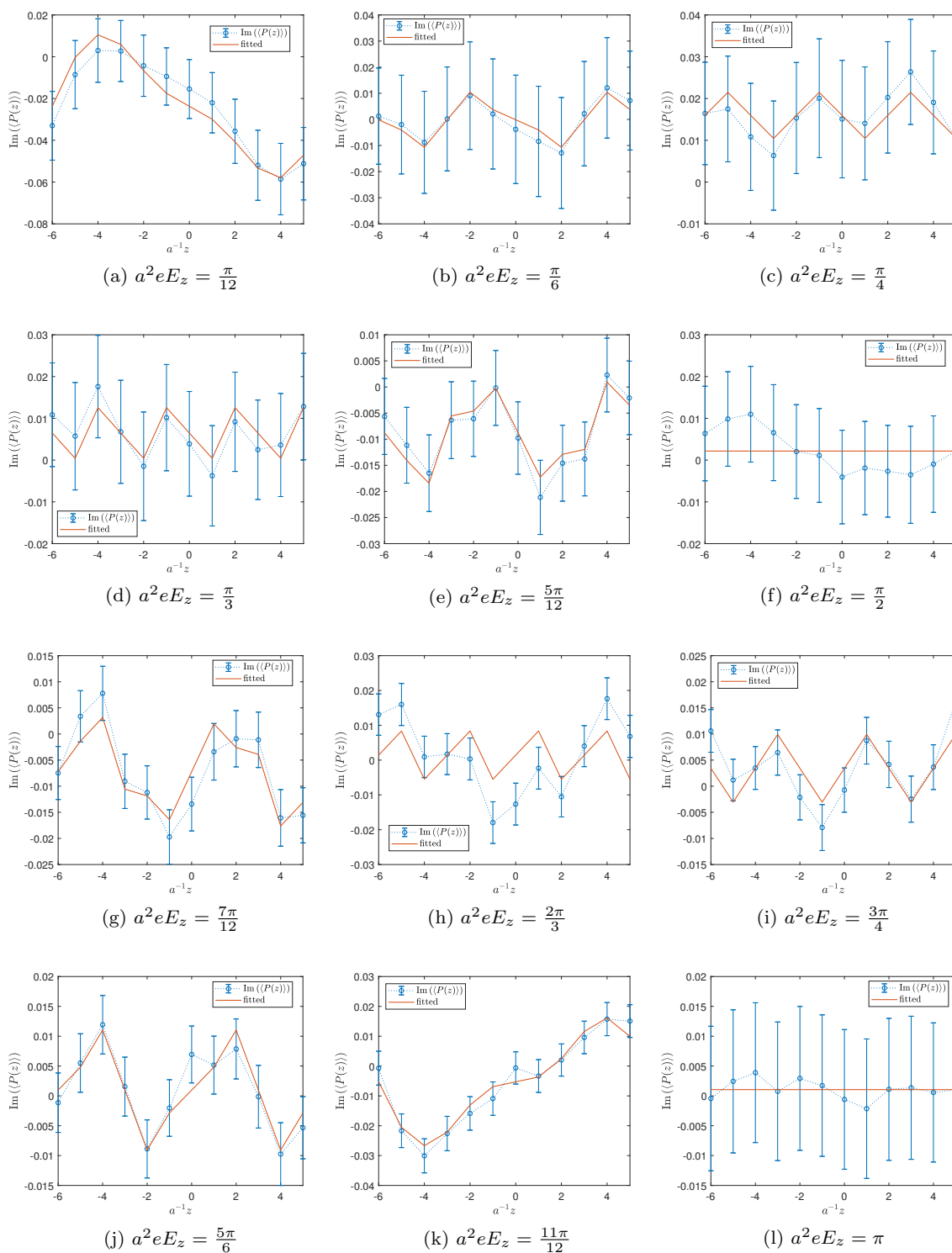


Figure 31. Same as figure 6 but for $\text{Im}(\langle P(z) \rangle)$ at $\beta = 5.42$.

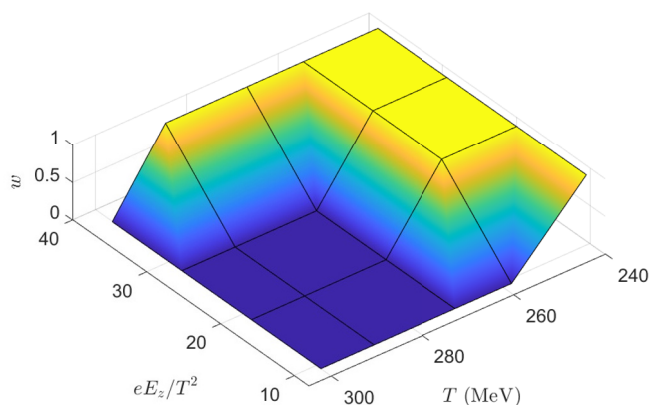


Figure 32. w as a function of T and eE_z/T^2 .

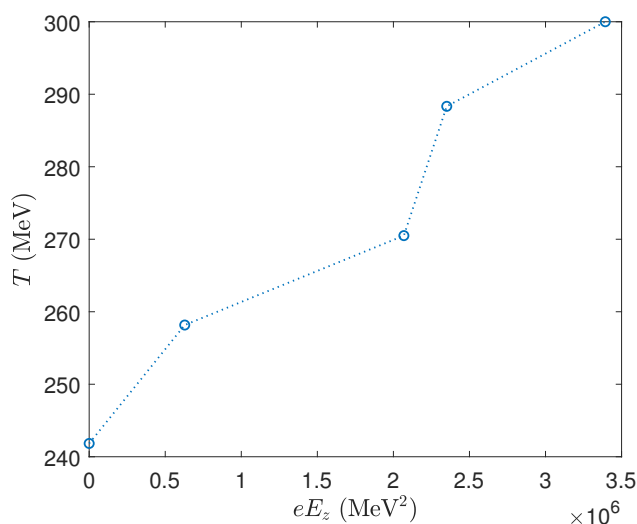


Figure 33. A boundary to distinguish the different behaviors of the Polyakov loop.

We use the winding number to distinguish different behaviors of the phases of Polyakov loops, which is defined as

$$w = -\frac{1}{2\pi i} \int_0^{2\pi} \frac{2iC_u \exp(2ix) - iC_d \exp(-ix)}{A_p + C_d \exp(-ix) + C_u \exp(2ix)} dx. \quad (3.15)$$

w is shown in figure 32. The case of $\beta = 5.38$ and $a^2 eE_z = \pi/12$ is special. The absolute value of the phase of $\langle P \rangle$ can exceed $\pi/2$ as shown in right panel of figure 21, not because in the complex plane, $\langle P \rangle$ encloses the origin, but because the two angles on the left side of the pointed triangle poke into the half plane where $\text{Re}[\langle P \rangle] < 0$.

Using $w \neq 0$ as a criterion, the boundary of possible transition can be obtained, which is shown in figure 33. Whether there is a phase transition needs more exploration. Note

that, this boundary also coincides with the boundary that the charge density start to oscillate as shown in figure 15.

4 Summary

The strong electric fields in heavy ion collisions provide a unique opportunity to study the effect of an external electromagnetic field on the quark matter. The case of classical electric field is considered which is free from the ‘sign problem’. In the case of \mathbf{E} along \mathbf{z} direction and in axial gauge, and neglecting the boundary condition, the electric field is equivalent as inhomogeneous imaginary chemical potential varies along the z coordinate.

In this paper, we investigate the properties of the R-W phase caused by an external uniform classical electric field using lattice QCD with $N_f = 1 + 1$ staggered fermions. In the simulation, $am_q = 0.1$ is a constant, and β ranges from 5.3 to 5.64. The simulation is carried out on a $12^3 \times 6$ lattice, $a^2 e E_z$ is chosen as $a^2 e E_z = k\pi/12$ where k is an integer and $0 \leq k \leq 12$.

It is found that, at high temperatures, chiral condensation oscillates over z coordinates. Note that the action is actually translational invariant accompanied by a gauge transformation. The oscillation over z coordinates partially breaks the translational invariance. c_q at high temperatures can be well-fitted by the ansatz $A_c + B_c \cos(iL_\tau a Q_q z e E_z)$. The analytical extension supports the conclusion that the chiral symmetry is restored by the external electric field. The charge density also oscillate over z coordinates with a same frequency. Apart from that, a weak signal of rho meson condensation is observed, but it is also possible that this is a fake phenomenon from discretization errors.

The imaginary part of the Polyakov loop shows up as expected, which indicates the presence of the R-W transition. At low temperatures and small electric field strength, the phase of Polyakov loop has plateaus at $2n\pi/3$. When the widths of plateaus are neglected, $\arg(\langle P(z) \rangle) \approx -2iazeE_z$. At high temperatures, the phase of the Polyakov loop is restricted to $(-\pi/2, \pi/2)$, and the absolute value of the phase decreases with the growth of temperature. Meanwhile, the absolute value of the Polyakov loop starts to oscillate over z coordinate.

It is verified that, the Polyakov loop can be described by ansatz $A_p + \sum_{q=u,d} B_q \exp(L_\tau ia Q_q z e E_z)$. From low temperature to high temperature, the size relation between $|A_p|$ and C_q changes, which results in different behavior of the Polyakov loop. The boundary to distinguish whether the Polyakov loop enclose the origin is obtained and is found to be close to the boundary that charge density starts to oscillate. Since the behavior of the phase of Polyakov loop is very different based on whether the origin is enclosed, there is a possible phase transition, at E_z much larger than the expected R-W transition or chiral transition.

Acknowledgments

We are grateful to Gergely Endrődi for useful discussions. This work was supported in part by the National Natural Science Foundation of China under Grants No. 12147214, the Nat-

ural Science Foundation of the Liaoning Scientific Committee No. LJKZ0978 and the Outstanding Research Cultivation Program of Liaoning Normal University (No. 21GDL004).

Open Access. This article is distributed under the terms of the Creative Commons Attribution License ([CC-BY 4.0](https://creativecommons.org/licenses/by/4.0/)), which permits any use, distribution and reproduction in any medium, provided the original author(s) and source are credited. SCOAP³ supports the goals of the International Year of Basic Sciences for Sustainable Development.

References

- [1] V.P. Gusynin, V.A. Miransky and I.A. Shovkovy, *Catalysis of dynamical flavor symmetry breaking by a magnetic field in (2+1)-dimensions*, *Phys. Rev. Lett.* **73** (1994) 3499 [Erratum *ibid.* **76** (1996) 1005] [[hep-ph/9405262](https://arxiv.org/abs/hep-ph/9405262)] [[INSPIRE](#)].
- [2] N.O. Agasian, *Phase structure of the QCD vacuum in a magnetic field at low temperature*, *Phys. Lett. B* **488** (2000) 39 [[hep-ph/0005300](https://arxiv.org/abs/hep-ph/0005300)] [[INSPIRE](#)].
- [3] I.A. Shovkovy, *Magnetic Catalysis: A Review*, *Lect. Notes Phys.* **871** (2013) 13 [[arXiv:1207.5081](https://arxiv.org/abs/1207.5081)] [[INSPIRE](#)].
- [4] G. Cao, *Recent progresses on QCD phases in a strong magnetic field: views from Nambu–Jona-Lasinio model*, *Eur. Phys. J. A* **57** (2021) 264 [[arXiv:2103.00456](https://arxiv.org/abs/2103.00456)] [[INSPIRE](#)].
- [5] H.T. Ding, S.T. Li, Q. Shi, A. Tomiya, X.D. Wang and Y. Zhang, *QCD phase structure in strong magnetic fields*, *Acta Phys. Polon. Supp.* **14** (2021) 403 [[arXiv:2011.04870](https://arxiv.org/abs/2011.04870)] [[INSPIRE](#)].
- [6] X.-G. Huang, *Electromagnetic fields and anomalous transports in heavy-ion collisions — A pedagogical review*, *Rept. Prog. Phys.* **79** (2016) 076302 [[arXiv:1509.04073](https://arxiv.org/abs/1509.04073)] [[INSPIRE](#)].
- [7] A.Y. Babansky, E.V. Gorbar and G.V. Shchepanyuk, *Chiral symmetry breaking in the Nambu–Jona-Lasinio model in external constant electromagnetic field*, *Phys. Lett. B* **419** (1998) 272 [[hep-th/9705218](https://arxiv.org/abs/hep-th/9705218)] [[INSPIRE](#)].
- [8] A. Goyal and M. Dahiya, *Chiral symmetry in linear sigma model in magnetic environment*, *Phys. Rev. D* **62** (2000) 025022 [[hep-ph/9906367](https://arxiv.org/abs/hep-ph/9906367)] [[INSPIRE](#)].
- [9] S.P. Klevansky, *The Nambu–Jona-Lasinio model of quantum chromodynamics*, *Rev. Mod. Phys.* **64** (1992) 649 [[INSPIRE](#)].
- [10] D. Ebert, K.G. Klimenko, M.A. Vdovichenko and A.S. Vshivtsev, *Magnetic oscillations in dense cold quark matter with four fermion interactions*, *Phys. Rev. D* **61** (2000) 025005 [[hep-ph/9905253](https://arxiv.org/abs/hep-ph/9905253)] [[INSPIRE](#)].
- [11] K.G. Klimenko and D. Ebert, *Magnetic catalysis of stability of quark matter in the Nambu–Jona-Lasinio model*, *Phys. Atom. Nucl.* **68** (2005) 124 [[INSPIRE](#)].
- [12] G.S. Bali et al., *The QCD phase diagram for external magnetic fields*, *JHEP* **02** (2012) 044 [[arXiv:1111.4956](https://arxiv.org/abs/1111.4956)] [[INSPIRE](#)].
- [13] G.S. Bali, F. Bruckmann, G. Endrodi, Z. Fodor, S.D. Katz and A. Schafer, *QCD quark condensate in external magnetic fields*, *Phys. Rev. D* **86** (2012) 071502 [[arXiv:1206.4205](https://arxiv.org/abs/1206.4205)] [[INSPIRE](#)].
- [14] G.S. Bali, F. Bruckmann, G. Endrodi, F. Gruber and A. Schaefer, *Magnetic field-induced gluonic (inverse) catalysis and pressure (an)isotropy in QCD*, *JHEP* **04** (2013) 130 [[arXiv:1303.1328](https://arxiv.org/abs/1303.1328)] [[INSPIRE](#)].

- [15] A. Tomiya, H.-T. Ding, S. Mukherjee, C. Schmidt and X.-D. Wang, *Chiral phase transition of three flavor QCD with nonzero magnetic field using standard staggered fermions*, *EPJ Web Conf.* **175** (2018) 07041 [[arXiv:1711.02884](#)] [[INSPIRE](#)].
- [16] A. Tomiya, H.-T. Ding, X.-D. Wang, Y. Zhang, S. Mukherjee and C. Schmidt, *Phase structure of three flavor QCD in external magnetic fields using HISQ fermions*, *PoS LATTICE2018* (2019) 163 [[arXiv:1904.01276](#)] [[INSPIRE](#)].
- [17] H.-T. Ding, S.-T. Li, S. Mukherjee, A. Tomiya and X.-D. Wang, *Meson masses in external magnetic fields with HISQ fermions*, *PoS LATTICE2019* (2020) 250 [[arXiv:2001.05322](#)] [[INSPIRE](#)].
- [18] H.T. Ding, S.T. Li, Q. Shi and X.D. Wang, *Fluctuations and correlations of net baryon number, electric charge and strangeness in a background magnetic field*, *Eur. Phys. J. A* **57** (2021) 202 [[arXiv:2104.06843](#)] [[INSPIRE](#)].
- [19] H.T. Ding, S.T. Li, J.H. Liu and X.D. Wang, *Chiral condensates and screening masses of neutral pseudoscalar mesons in thermomagnetic QCD medium*, *Phys. Rev. D* **105** (2022) 034514 [[arXiv:2201.02349](#)] [[INSPIRE](#)].
- [20] M. D'Elia, *Lattice QCD Simulations in External Background Fields*, *Lect. Notes Phys.* **871** (2013) 181 [[arXiv:1209.0374](#)] [[INSPIRE](#)].
- [21] S. Mao, *From inverse to delayed magnetic catalysis in a strong magnetic field*, *Phys. Rev. D* **94** (2016) 036007 [[arXiv:1605.04526](#)] [[INSPIRE](#)].
- [22] M.N. Chernodub, *QCD string breaking in strong magnetic field*, *Mod. Phys. Lett. A* **29** (2014) 1450162 [[arXiv:1001.0570](#)] [[INSPIRE](#)].
- [23] M. Ferreira, P. Costa, O. Lourenço, T. Frederico and C. Providência, *Inverse magnetic catalysis in the (2+1)-flavor Nambu-Jona-Lasinio and Polyakov-Nambu-Jona-Lasinio models*, *Phys. Rev. D* **89** (2014) 116011 [[arXiv:1404.5577](#)] [[INSPIRE](#)].
- [24] J. Chao, P. Chu and M. Huang, *Inverse magnetic catalysis induced by sphalerons*, *Phys. Rev. D* **88** (2013) 054009 [[arXiv:1305.1100](#)] [[INSPIRE](#)].
- [25] A. Bazavov et al., *Freeze-out Conditions in Heavy Ion Collisions from QCD Thermodynamics*, *Phys. Rev. Lett.* **109** (2012) 192302 [[arXiv:1208.1220](#)] [[INSPIRE](#)].
- [26] K. Fukushima and Y. Hidaka, *Magnetic Catalysis Versus Magnetic Inhibition*, *Phys. Rev. Lett.* **110** (2013) 031601 [[arXiv:1209.1319](#)] [[INSPIRE](#)].
- [27] F. Bruckmann, G. Endrodi and T.G. Kovacs, *Inverse magnetic catalysis and the Polyakov loop*, *JHEP* **04** (2013) 112 [[arXiv:1303.3972](#)] [[INSPIRE](#)].
- [28] M.A. Nowak, M. Sadzikowski and I. Zahed, *Chiral Disorder and Random Matrix Theory with Magnetism*, *Acta Phys. Polon. B* **47** (2016) 2173 [[arXiv:1304.6020](#)] [[INSPIRE](#)].
- [29] L. Yu, H. Liu and M. Huang, *Spontaneous generation of local CP-violation and inverse magnetic catalysis*, *Phys. Rev. D* **90** (2014) 074009 [[arXiv:1404.6969](#)] [[INSPIRE](#)].
- [30] H. Liu, L. Yu and M. Huang, *Charged and neutral vector ρ mesons in a magnetic field*, *Phys. Rev. D* **91** (2015) 014017 [[arXiv:1408.1318](#)] [[INSPIRE](#)].
- [31] H. Liu, X. Wang, L. Yu and M. Huang, *Neutral and charged scalar mesons, pseudoscalar mesons, and diquarks in magnetic fields*, *Phys. Rev. D* **97** (2018) 076008 [[arXiv:1801.02174](#)] [[INSPIRE](#)].
- [32] A. Bzdak and V. Skokov, *Event-by-event fluctuations of magnetic and electric fields in heavy ion collisions*, *Phys. Lett. B* **710** (2012) 171 [[arXiv:1111.1949](#)] [[INSPIRE](#)].

- [33] W.-T. Deng and X.-G. Huang, *Event-by-event generation of electromagnetic fields in heavy-ion collisions*, *Phys. Rev. C* **85** (2012) 044907 [[arXiv:1201.5108](#)] [[INSPIRE](#)].
- [34] J. Błoczyński, X.-G. Huang, X. Zhang and J. Liao, *Azimuthally fluctuating magnetic field and its impacts on observables in heavy-ion collisions*, *Phys. Lett. B* **718** (2013) 1529 [[arXiv:1209.6594](#)] [[INSPIRE](#)].
- [35] S.P. Klevansky and R.H. Lemmer, *Chiral symmetry restoration in the Nambu-Jona-Lasinio model with a constant electromagnetic field*, *Phys. Rev. D* **39** (1989) 3478 [[INSPIRE](#)].
- [36] H. Suganuma and T. Tatsumi, *On the Behavior of Symmetry and Phase Transitions in a Strong Electromagnetic Field*, *Annals Phys.* **208** (1991) 470 [[INSPIRE](#)].
- [37] W.R. Tavares, R.L.S. Farias and S.S. Avancini, *Deconfinement and chiral phase transitions in quark matter with a strong electric field*, *Phys. Rev. D* **101** (2020) 016017 [[arXiv:1912.00305](#)] [[INSPIRE](#)].
- [38] G. Cao and X.-G. Huang, *Chiral phase transition and Schwinger mechanism in a pure electric field*, *Phys. Rev. D* **93** (2016) 016007 [[arXiv:1510.05125](#)] [[INSPIRE](#)].
- [39] M. Ruggieri, Z.Y. Lu and G.X. Peng, *Influence of chiral chemical potential, parallel electric, and magnetic fields on the critical temperature of QCD*, *Phys. Rev. D* **94** (2016) 116003 [[arXiv:1608.08310](#)] [[INSPIRE](#)].
- [40] M. Ruggieri and G.-X. Peng, *Chiral phase transition of quark matter in the background of parallel electric and magnetic fields*, *Nucl. Sci. Tech.* **27** (2016) 130 [[INSPIRE](#)].
- [41] A. Yamamoto, *Lattice QCD with strong external electric fields*, *Phys. Rev. Lett.* **110** (2013) 112001 [[arXiv:1210.8250](#)] [[INSPIRE](#)].
- [42] P. de Forcrand and O. Philipsen, *The QCD phase diagram for small densities from imaginary chemical potential*, *Nucl. Phys. B* **642** (2002) 290 [[hep-lat/0205016](#)] [[INSPIRE](#)].
- [43] M. D'Elia and M.-P. Lombardo, *Finite density QCD via imaginary chemical potential*, *Phys. Rev. D* **67** (2003) 014505 [[hep-lat/0209146](#)] [[INSPIRE](#)].
- [44] E. Shintani et al., *Neutron electric dipole moment with external electric field method in lattice QCD*, *Phys. Rev. D* **75** (2007) 034507 [[hep-lat/0611032](#)] [[INSPIRE](#)].
- [45] A. Alexandru and F.X. Lee, *The Background field method on the lattice*, *PoS LATTICE2008* (2008) 145 [[arXiv:0810.2833](#)] [[INSPIRE](#)].
- [46] M. D'Elia, M. Mariti and F. Negro, *Susceptibility of the QCD vacuum to CP-odd electromagnetic background fields*, *Phys. Rev. Lett.* **110** (2013) 082002 [[arXiv:1209.0722](#)] [[INSPIRE](#)].
- [47] H.R. Fiebig, W. Wilcox and R.M. Woloshyn, *A Study of Hadron Electric Polarizability in Quenched Lattice QCD*, *Nucl. Phys. B* **324** (1989) 47 [[INSPIRE](#)].
- [48] J.C. Christensen, W. Wilcox, F.X. Lee and L.-m. Zhou, *Electric polarizability of neutral hadrons from lattice QCD*, *Phys. Rev. D* **72** (2005) 034503 [[hep-lat/0408024](#)] [[INSPIRE](#)].
- [49] LHPC collaboration, *Neutron electric polarizability from unquenched lattice QCD using the background field approach*, *Phys. Rev. D* **76** (2007) 114502 [[arXiv:0706.3919](#)] [[INSPIRE](#)].
- [50] G. Endrodi and G. Marko, *Thermal QCD with external imaginary electric fields on the lattice*, *PoS LATTICE2021* (2022) 245 [[arXiv:2110.12189](#)] [[INSPIRE](#)].
- [51] G. Endródi and G. Markó, *On electric fields in hot QCD: perturbation theory*, [arXiv:2208.14306](#) [[INSPIRE](#)].

- [52] A. Roberge and N. Weiss, *Gauge Theories With Imaginary Chemical Potential and the Phases of QCD*, *Nucl. Phys. B* **275** (1986) 734 [INSPIRE].
- [53] O. Philipsen and C. Pinke, *Nature of the Roberge-Weiss transition in $N_f = 2$ QCD with Wilson fermions*, *Phys. Rev. D* **89** (2014) 094504 [arXiv:1402.0838] [INSPIRE].
- [54] M. D’Elia and M. Mariti, *Effect of Compactified Dimensions and Background Magnetic Fields on the Phase Structure of $SU(N)$ Gauge Theories*, *Phys. Rev. Lett.* **118** (2017) 172001 [arXiv:1612.07752] [INSPIRE].
- [55] J. Samuel, *Wick Rotation in the Tangent Space*, *Class. Quant. Grav.* **33** (2016) 015006 [arXiv:1510.07365] [INSPIRE].
- [56] J.B. Kogut and L. Susskind, *Hamiltonian Formulation of Wilson’s Lattice Gauge Theories*, *Phys. Rev. D* **11** (1975) 395 [INSPIRE].
- [57] C. Gattringer and C.B. Lang, *Quantum chromodynamics on the lattice*, vol. 788, Springer, Berlin (2010), 10.1007/978-3-642-01850-3 [INSPIRE].
- [58] K.G. Wilson, *Confinement of Quarks*, *Phys. Rev. D* **10** (1974) 2445 [INSPIRE].
- [59] P.H. Damgaard and U.M. Heller, *The $U(1)$ Higgs Model in an External Electromagnetic Field*, *Nucl. Phys. B* **309** (1988) 625 [INSPIRE].
- [60] M.H. Al-Hashimi and U.J. Wiese, *Discrete Accidental Symmetry for a Particle in a Constant Magnetic Field on a Torus*, *Annals Phys.* **324** (2009) 343 [arXiv:0807.0630] [INSPIRE].
- [61] P.V. Buividovich, M.N. Chernodub, E.V. Luschevskaya and M.I. Polikarpov, *Lattice QCD in strong magnetic fields*, *eCONF C* **0906083** (2009) 25 [arXiv:0909.1808] [INSPIRE].
- [62] S. Ueda et al., *Development of an object oriented lattice QCD code ‘Bridge++’*, *J. Phys. Conf. Ser.* **523** (2014) 012046 [INSPIRE].
- [63] B. Orth, T. Lippert and K. Schilling, *Finite-size effects in lattice QCD with dynamical Wilson fermions*, *Phys. Rev. D* **72** (2005) 014503 [hep-lat/0503016] [INSPIRE].
- [64] TXL, T(X)L collaboration, *Static potentials and glueball masses from QCD simulations with Wilson sea quarks*, *Phys. Rev. D* **62** (2000) 054503 [hep-lat/0003012] [INSPIRE].
- [65] G.S. Bali and K. Schilling, *Static quark - anti-quark potential: Scaling behavior and finite size effects in $SU(3)$ lattice gauge theory*, *Phys. Rev. D* **46** (1992) 2636 [INSPIRE].
- [66] R. Sommer, *A New way to set the energy scale in lattice gauge theories and its applications to the static force and α_s in $SU(2)$ Yang-Mills theory*, *Nucl. Phys. B* **411** (1994) 839 [hep-lat/9310022] [INSPIRE].
- [67] M. Cheng et al., *The QCD equation of state with almost physical quark masses*, *Phys. Rev. D* **77** (2008) 014511 [arXiv:0710.0354] [INSPIRE].
- [68] MILC collaboration, *Results for light pseudoscalar mesons*, *PoS LATTICE2010* (2010) 074 [arXiv:1012.0868] [INSPIRE].
- [69] ALPHA collaboration, *Monte Carlo errors with less errors*, *Comput. Phys. Commun.* **156** (2004) 143 [Erratum *ibid.* **176** (2007) 383] [hep-lat/0306017] [INSPIRE].
- [70] A. Bazavov et al., *The chiral and deconfinement aspects of the QCD transition*, *Phys. Rev. D* **85** (2012) 054503 [arXiv:1111.1710] [INSPIRE].